Synoptic-Scale Atmospheric Circulation and Boreal Canada Summer Drought Variability of the Past Three Centuries

MARTIN-PHILIPPE GIRARDIN* AND JACQUES C. TARDIF

Centre for Forest Interdisciplinary Research, University of Winnipeg, Winnipeg, Manitoba, Canada

MIKE D. FLANNIGAN

Natural Resources Canada, Canadian Forest Service, Sault Sainte Marie, Ontario, Canada

YVES BERGERON

Groupe de Recherche en Écologie Forestière Inter-Universitaire, Université du Québec à Montréal, Montreal, Quebec, Canada

(Manuscript received 4 January 2005, in final form 30 September 2005)

ABSTRACT

Five independent multicentury reconstructions of the July Canadian Drought Code and one reconstruction of the mean July–August temperature were developed using a network of 120 well-replicated tree-ring chronologies covering the area of the eastern Boreal Plains to the eastern Boreal Shield of Canada. The reconstructions were performed using 54 time-varying reconstruction submodels that explained up to 50% of the regional drought variance during the period of 1919–84. Spatial correlation fields on the six reconstructions revealed that the meridional component of the climate system from central to eastern Canada increased since the mid–nineteenth century. The most obvious change was observed in the decadal scale of variability. Using 500-hPa geopotential height and wind composites, this zonal to meridional transition was interpreted as a response to an amplification of long waves flowing over the eastern North Pacific into boreal Canada, from approximately 1851 to 1940. Composites with NOAA Extended Reconstructed SSTs indicated a coupling between the meridional component and tropical and North Pacific SST for a period covering at least the past 150 yr, supporting previous findings of a summertime global ocean–atmosphere–land surface coupling. This change in the global atmospheric circulation could be a key element toward understanding the observed temporal changes in the Canadian boreal forest fire regimes over the past 150 yr.

1. Introduction

Forest fires are responsible for the spatial and temporal variations in the forest mosaic of the boreal forest (Bourgeau-Chavez et al. 2000). Fire has been an integral ecological process since the arrival of vegetation on the landscape. Weather and climate are important determinants of fire activity (Flannigan and Harrington 1988; Johnson 1992; Flannigan and Wotton 2001). In particular, the frequency of precipitation through the fire season rather than the amount of precipitation is a critical aspect of the weather in terms of fire activity. A low frequency of precipitation is associated with a high probability of a large burned area, and vice versa (Flannigan and Harrington 1988; Flannigan and Van Wagner 1991). Another key weather aspect is blocking ridges in the upper atmosphere. Most of the area burned in the boreal forest of Canada is attributed to large-blocking high pressure systems at the 500-hPa atmospheric pressure level that cause dry fuel conditions (Skinner et al. 1999, 2002; Flannigan and Wotton 2001). When high pressure systems begin to break down, convective activity leading to numerous lightning strikes occurs and this ignites forest fires (Nash and Johnson 1996).

Climate and the associated weather are always

* Current affiliation: Natural Resources Canada, Canadian Forest Service, Laurentian Forestry Centre, Quebec City, Quebec, Canada.

Corresponding author address: Martin-Philippe Girardin, Canadian Forest Service, Laurentian Forestry Centre, 1055, rue du P.E.P.S., C.P. 10380, Stn. Sainte-Foy, Quebec City, QC G1V 4C7, Canada.
E-mail: martin.girardin@rncan.gc.ca

changing because of a number of factors such as solar variability, changes in the chemical composition of the atmosphere, and volcanoes. Thus, with a dynamic climate and the strong linkage between climate and forest fires, variations in historical observations of fire activity resulting from changes in the climate and weather are expected. Studies have suggested that the fire regime in the Canadian boreal forest changed after the end of the Little Ice Age (~1850). The age distributions of forest stands across large areas of the Canadian boreal forest, reconstructed from living trees, snags, and downed woody material, suggest that fire frequency and the area burned have significantly diminished since 1850 (Larsen 1996; Weir et al. 2000; Bergeron et al. 2001; Bergeron et al. 2004). The existence of a trend toward a more moist climate in eastern boreal Canada was further documented in studies of forest communities located in flood-prone environments (Tardif and Bergeron 1997a; Tardif and Bergeron 1999), which revealed an increase in the frequency and magnitude of spring water levels at ice breakup. This trend agrees with studies made in the Canadian Plains. Salinity reconstructions in Alberta revealed that past aridity severity (1300–1750 period) was generally greater than that recorded during the instrumental period (Sauchyn et al. 2002). While drought was frequent in the twentieth century, it tended to be of short duration and was separated by periods of relatively high precipitation (Sauchyn et al. 2003). With respect to fire weather severity under a $2 \times CO_2$ scenario, general circulation model (GCM) simulations predict a trend toward a moister climate in the Boreal Shield, and a drier climate in the Great Plains (Flannigan and Wotton 2001). This agrees with other simulations suggesting more intense, more frequent, and longer lasting 500-hPa-blocking high pressure systems over western-central North America, resulting from ongoing increases in greenhouse gases (Meehl and Tebaldi 2004).

Because of the relationship between atmospheric circulation and area burned, it was hypothesized that historical changes in the boreal forest fire regime were attributed to changes in the circulation of air masses (Bergeron and Archambault 1993; Hofgaard et al. 1999) and sea surface temperatures (SSTs; Girardin et al. 2004a). Ocean and atmosphere summertime couplings over Canada have been addressed and recognized by many authors (Bonsal et al. 1993; Bonsal and Lawford 1999; Nigam et al. 1999; Barlow et al. 2001; Girardin et al. 2004a,b; Shabbar and Skinner 2004). Nevertheless, most climate studies are based on short-term data and can provide little or no information on past climate history and its influence on vegetation dynamics. Therefore, this paper investigates the spatial and temporal variations observed in summer drought severity during the last three centuries in the eastern Boreal Plains and Boreal Shield of Canada. The extent to which the variability in the proxy records reflects changes in atmospheric and oceanic circulation is also explored.

2. Data and methods

Six independent annually resolved climate reconstructions going back to the early 1700s that are representative of climate variability from the eastern Boreal Plains to the eastern Boreal Shield were developed from a dense network of 120 tree-ring chronologies. Five of these were reconstructions of the July Canadian Drought Code (CDC; Turner 1972; Girardin et al. 2004a). The sixth was a reconstruction of the mean July–August temperature. The dynamics between drought variability and atmospheric and oceanic drivers was analyzed using the National Centers for Environmental Prediction–National Center for Atmospheric Research (NCEP–NCAR) reanalysis gridded instrumental 500-hPa geopotential heights and vector winds (1948–84; Kalnay et al. 1996), and National Oceanic and Atmospheric Administration (NOAA) Extended Reconstructed Sea Surface Temperatures (ERSST; 1854–84 period; Smith and Reynolds 2003).

a. Study area

The study area covers the eastern Boreal Plains to the eastern Boreal Shield ecozones, and most of the boreal forest from western Manitoba to eastern Quebec (Fig. 1). The study area covers six climate regions (Fig. 1), with boundaries approximating actual ecoregions defined by the Ecological Stratification Working Group (1996). These climate regions are the Boreal Plains (BP), Lac Seul Upland and Lake of the Woods (LS), Lake Nipigon (LN), the west and east Abitibi Plains (APw and APe, respectively), and southern Laurentian (SL) (Fig. 1).

All six regions under study have a subhumid to humid midboreal ecoclimate (west–east gradient), marked by warm summers and cold, snowy winters according to the Ecological Stratification Working Group's (1996) regional classification. In the BP and LS regions, the average annual temperature ranges between −1.0° and 1.0°C, whereas eastern regions from LN to SL range between 1.0° and 1.5°C. The average summer temperature is similar across the six regions, approximately 14.0°C. The average winter temperatures are more variable, ranging from −16.0°C in the BP region to −11.0°C in the SL region. The average

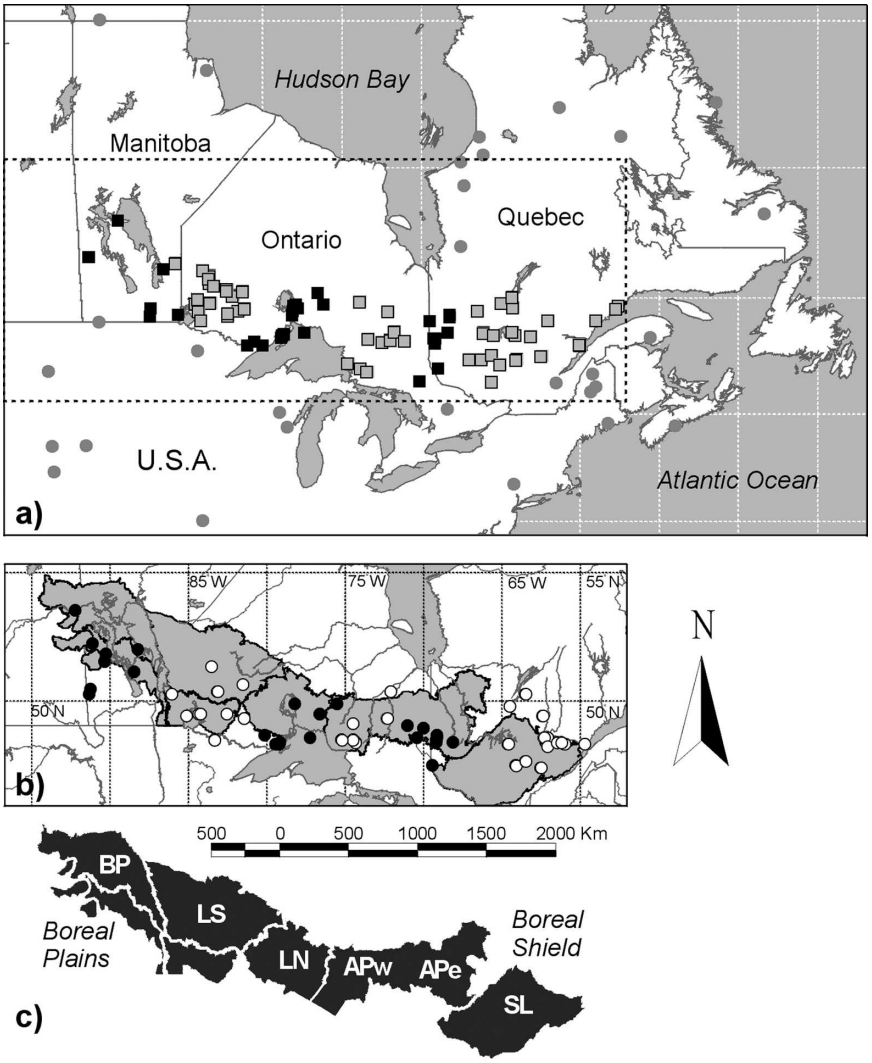

FIG. 1. (a) Geographical distribution of the locations of the 120 residual tree-ring chronologies used for the climate reconstructions (squares). The different shades delineated the six regions. Supplemental chronologies used in a spatiotemporal analysis of radial growth are shown with circles (refer to section 3g). (b) Geographical distribution of the locations of the meteorological stations used in the calculation of the regional climate variables. (c) Domain of the area under study. Six regions enclosed by the shaded areas were selected for the climate reconstruction: BP, LS, LN, APw, APe, and SL.

annual precipitation ranges from 450 mm in the west to 1600 mm in the east. Most of the annual precipitation in the study area falls between the months of June and October (Environment Canada 2002).

b. Development of the tree-ring residual chronologies

In winter 2001, a survey of available ring-width measurement series was made for the construction of a tree-ring chronology network. Sixty-three datasets were gathered from the International Tree Ring Data Bank (ITRDB) data library (Archambault and Bergeron 1992; Hofgaard et al. 1999; Tardif and Bergeron 1997b; Jardon et al. 2003; Girardin et al. 2004a; Girardin and Tardif 2005). In 2002 and 2003, sampling was conducted in Ontario to fill gaps within the network; 57 datasets were collected. Tree-rings were sampled and cross dated using standard techniques (Yamaguchi 1991; Girardin and Tardif 2005) and were validated using the COFECHA program (Holmes 1983).

In total, 120 datasets of ring-width measurement series from 13 species and extending back to at least 1866

were gathered for dendroclimatic reconstruction (Fig. 1; appendix A). The major species were conifers of the genus *Pinus* (45% of all datasets), with the exception of the Quebec area in which the genus *Picea* represented 51% of all datasets. The species *Thuja occidentalis* L. also represented an important fraction of the datasets (15%). In general, the datasets were well replicated, with only 13% of them being composed of less than 30 measurement series (appendix A). At least 25 chronologies had high subsample signal strength for a period covering the late-eighteenth century to present.

The age-/size-related trend was removed from the tree-ring measurement series using a spline function giving a 50% frequency response of 60 yr (Cook and Peters 1981). Although this detrending procedure resulted in the loss of information relative to long-term climate changes, 99% of the variance contained in frequencies lower than 19 yr was preserved. This "flexible" smoothing was necessary because many of the tree-ring series were less than 100 yr in length. The biological persistence contained in the standardized measurement series was removed (autoregressive modeling) to eliminate variation not resulting from climate (Cook and Holmes 1986). Biweight robust means of the residual measurement series were computed to create the residual chronologies. All chronologies were constructed using the ARSTAN program (Holmes 1999).

c. Development of the climate data

Analyses of the tree growth–climate relationships were conducted using regional mean monthly average CDC (a description follows) from Girardin et al. (2004b), mean monthly temperature from Vincent and Gullett (1999), and total monthly precipitation from Mekis and Hogg (1999). The MET program from the Dendrochronology Program Library (Holmes 1999) was used to estimate the missing data for each station and to combine the stations into regional variables. Monthly variables for each station were normalized to give each station the same weight in calculating the mean values for each month and year. (Refer to Fig. 1b for the distribution of stations and to appendix B for a list of stations.)

The CDC is a daily component of the Fire Weather Index System (Van Wagner 1987) that is used across Canada by fire management agencies to monitor forest fire danger. It is an indicator of summertime moisture in deep organic layers in boreal conifer stands (Van Wagner 1970) and correlates well with radial growth of numerous boreal tree species (Bergeron and Archambault 1993; Tardif and Bergeron 1997b; Girardin et al. 2004a; Girardin and Tardif 2005). Moisture losses in the CDC are the result of daily evaporation and transpiration, while daily precipitation accounts for moisture gains. Evaporation and transpiration losses are first estimated as a maximum potential evapotranspiration based on temperature and seasonal day length. Second, this maximum potential evapotranspiration value is scaled by the available soil moisture to reflect the fact that as soil moisture content is reduced, evaporation is increasingly difficult (Turner 1972). The maximum water-holding capacity of the CDC is 100 mm for a layer with a bulk density of about 25 kg m^{-2}, which amounts to approximately 400% of water per unit of mass. The minimum CDC value of zero represents soil saturation. A CDC rating of 200 indicates high drought and a rating above 300 indicates severe drought. Refer to Girardin et al. (2004b) and Girardin (2005) for further details.

d. Tree growth and climate relationships

Redundancy analysis (RDA) (Legendre and Legendre 1998; Tardif et al. 2003; Girardin et al. 2004a) was used to investigate the species' response to climate. RDA is the canonical extension of principal component analysis (PCA) and displays the main trends in variation of a multidimensional dataset in a reduced space of a few linearly independent dimensions. In RDA, the canonical axes differ from the principal components (PCs) in that they are constrained to be linear combinations of supplied environmental variables (Ter Braak and Prentice 1988; Ter Braak 1994). RDA may be understood as a two-step process: (i) each residual chronology is regressed on the selected climate variables and the predicted values are computed, and (ii) a PCA is then carried out on the matrix of predicted values to obtain the eigenvalues and eigenvectors (Legendre and Legendre 1998). The climate variables were selected using a forward selection on the basis of the goodness of fit and were tested for significance at the 5% level using 999 Monte Carlo unrestricted permutations.

One RDA was computed from each of the six regions. The dependent-variables dataset included all residual chronologies for a given climate region and the independent-variables dataset included the corresponding regional mean monthly CDC, mean monthly temperature, and total monthly precipitation. All analyses were constrained to the common interval of 1919–84 because of the availability of meteorological data in the earliest years and of chronologies in the latest years. The period of analysis included from June of the year previous to ring formation to September of the year of ring formation. All RDA were conducted on covariance matrices because the descriptors (the tree-ring chronologies) were of the same kind, shared the same order of magnitude, and were measured in the same

units (Legendre and Legendre 1998). RDA was computed using the CANOCO 4.0 program (Ter Braak and Smilauer 1998), and the scaling of ordination scores was done using correlation biplots.

e. Reconstruction of drought severity

The climate reconstructions were performed using the varying time series technique described by Cook et al. (2002), Luterbacher et al. (2002), and Girardin et al. (2004a). Because of large time-varying chronologies, 54 submodels were developed for the reconstructions. The number of submodels constructed for each region varied between 6 and 11, starting with a minimum of five chronologies and adding chronologies in subsequent submodels. In each reconstruction submodel, the available residual chronologies were transformed into nonrotated PCs to remove multicollinearity (Cook and Kairiukstis 1990; Legendre and Legendre 1998). Up to four PCs were kept for calibration. Because tree growth in the year of ring formation is influenced by weather conditions in both the current and the prior growing seasons (e.g., Archambault and Bergeron 1992; Hofgaard et al. 1999; Fritts 2001; Girardin and Tardif 2005), the four PCs were also forwarded by 1 yr and included in the calibrations. PCA were conducted on covariance matrices and CANOCO 4.0 was used (Ter Braak and Smilauer 1998).

Calibrations for the period of 1919–84 were conducted on the predictors using forward stepwise multiple linear regression analyses between the instrumental climate indices (predictands) and the PCs (predictors; present and forward lags) (Cook and Kairiukstis 1990). The yearly climate indices for the early period covered by the site residual chronologies were estimated from the calibration equations. The stability of each submodel was verified as follows (Woodhouse 2003). The predictors selected from the 1919–84 calibration were used in a regression equation to predict drought in the period of 1941–84, and the resulting equation was tested on the period of 1919–40. The strength of the relationship between reconstruction and observation over the verification period of 1919–40 was measured by the reduction of error (RE) discussed in Cook et al. (1994). The RE provides a sensitive measure of reconstruction reliability. Whenever RE is greater than zero the reconstruction is considered as being a better estimation of climate than the calibration period mean. The final reconstructions were built after merging segments of the submodels.

f. Atmospheric circulation

The long-term history of atmospheric circulation was analyzed using the nonrotated PCA approach (Yarnal 1993) on correlation matrices of drought reconstructions. Large-scale correlation structure over the area is likely to relate to the large-scale atmospheric circulation, and therefore PCA is an appropriate tool to find patterns of variability that may be linked to atmospheric circulation. A correlation matrix was used so that all descriptors could contribute equally to the clustering of objects, independent of the variance (and units) exhibited by each one (Legendre and Legendre 1998).

Continuous wavelet transform (CWT) analyses were conducted to identify nonstationary signals in the first and second PCs of the six reconstructions. CWT was used to decompose signals into wavelets (small oscillations that are highly localized in time; Torrence and Compo 1998). CWT analyses were performed using the Morlet wavelet basis with a wavenumber of 6 (AISN Software 1999).

The atmosphere's physical dynamics were analyzed using May–July seasonal means of 500-hPa NCEP–NCAR reanalysis geopotential height (m) and vector wind ($m\ s^{-1}$) composites. The NCEP–NCAR reanalysis 500-hPa grid has a global spatial coverage of 2.5° latitude × 2.5° longitude with 144 × 73 points and a temporal coverage from 1948 to the present (Kalnay et al. 1996). SST composites were also created using NOAA ERSST (from Smith and Reynolds 2003). The ERSST covers the period from 1854 to the present. All maps were created with the aid of the National Oceanic and Atmospheric Administration–Cooperative Institute for Research in Environmental Sciences (NOAA–CIRES) Climate Diagnostics Center, in Boulder, Colorado (see information available online at http://www.cdc.noaa.gov).

3. Results

a. Tree-ring width and climate relationships

The RDA eigenvectors indicated that the majority of chronologies within their respective climate regions shared common environmental signals (Fig. 2). This was particularly true for the APw and SL regions in which the first canonical axis alone explained at least 25% of the total variance (Table 1). The partitioning of the chronologies was particularly strong on the positive side of the first eigenvector, with 60.8% of the chronologies having an eigenvector loading greater than 0.40. Only 5.8% of the chronologies had a similar loading on eigenvector 2 and a tendency for a distribution of *Betula papyrifera* Marsh. and *Quercus macrocarpa* Michx. along the second eigenvector was observed. Clustering of species within the reduced space was also observed, particularly with *Pinus resinosa* Ait. and *Pi-*

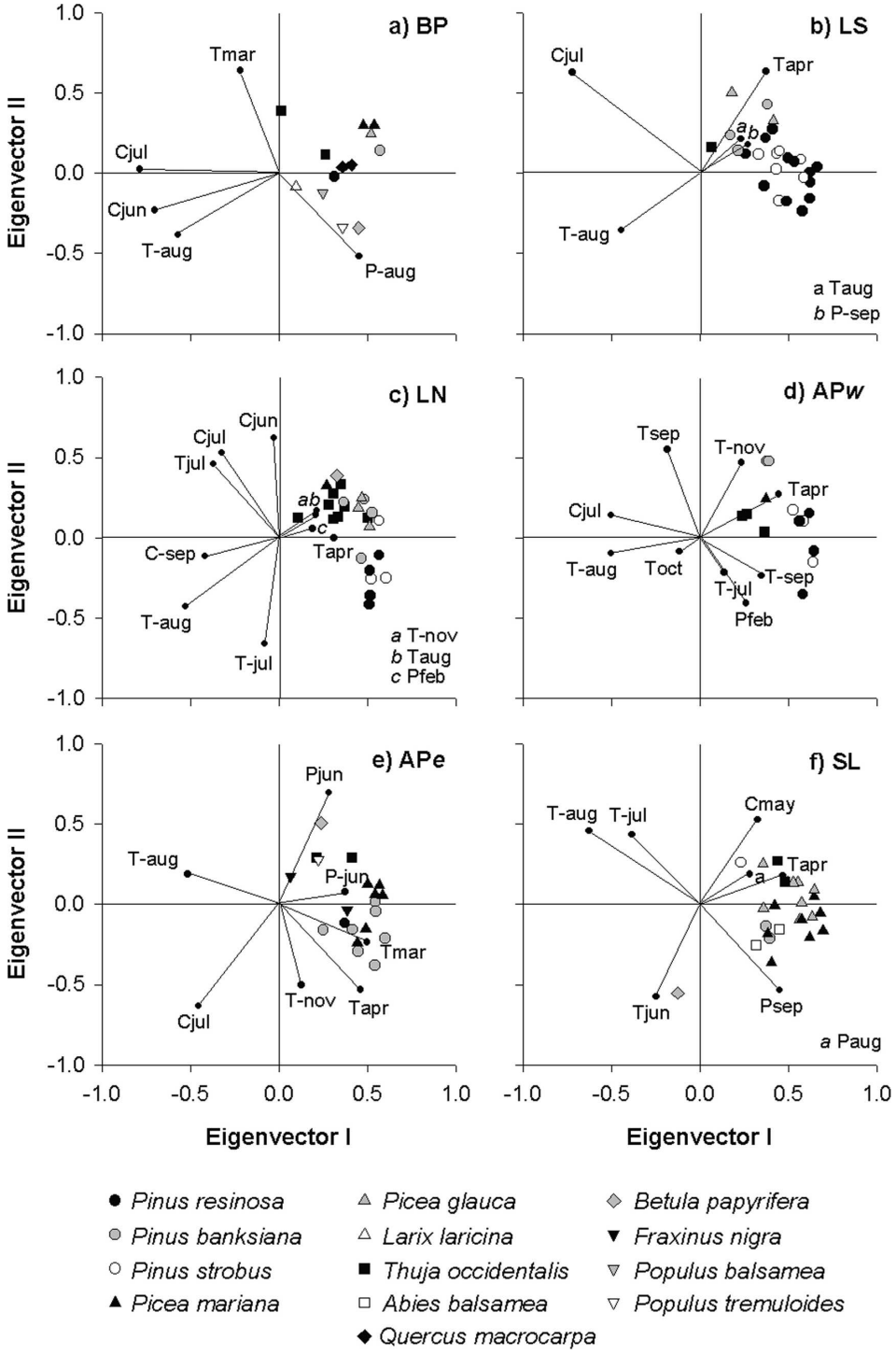

FIG. 2. Eigenvectors of the RDA conducted on the site residual chronologies for the six regions. For clarity, arrows pointing from the origin to the descriptors (species chronologies) were not drawn. The descriptors are positioned in the biplot based on their correlations with the canonical axes. In addition, the biplot also approximates the correlation coefficient among descriptors and climate variables (Legendre and Legendre 1998). Climate variables and residual chronologies with "arrows" at sharp angles are positively correlated ($\cos 0° = 1.0$, i.e., perfect correlation). Conversely, obtuse angles indicate negative correlation ($\cos 180° = -1.0$, i.e., perfect correlation). Climate variable abbreviations are for temperature (T), precipitation (P), and CDC (C). Months range from July of the year prior (−jul) to September of the year current (sep) to ring formation. Statistics of the RDA are given in Table 1. The significance of all canonical axes is $p < 0.001$.

TABLE 1. Redundancy analyses statistics per climate region.

	Canonical axis 1	Canonical axis 2
Boreal Plains		
Eigenvalues[a]	0.15	0.05
Species–environment correlations[b]	0.68	0.55
Cumulative percentage variance of species–environment relation (%)[c]	63.20	85.10
Lac Seul and Lake of the Woods		
Eigenvalues[a]	0.23	0.03
Species–environment correlations[b]	0.70	0.58
Cumulative percentage variance of species–environment relation (%)[c]	81.00	92.10
Lake Nipigon		
Eigenvalues[a]	0.21	0.07
Species–environment correlations[b]	0.82	0.71
Cumulative percentage variance of species–environment relation (%)[c]	56.70	75.50
Abitibi Plains west		
Eigenvalues[a]	0.28	0.07
Species–environment correlations[b]	0.78	0.69
Cumulative percentage variance of species–environment relation (%)[c]	68.40	86.00
Abitibi Plains east		
Eigenvalues [a]	0.18	0.07
Species–environment correlations[b]	0.76	0.68
Cumulative percentage variance of species–environment relation (%)[c]	58.40	79.80
Southern Laurentian		
Eigenvalues[a]	0.25	0.04
Species–environment correlations[b]	0.77	0.69
Cumulative percentage variance of species–environment relation (%)[c]	75.20	87.80

[a] Variance in a set of variables explained by a canonical axis.
[b] Amount of the variation in species composition that may be "explained" by the environmental variables.
[c] Amount of variance explained by the canonical axes as a fraction of the total explainable variance.

nus strobus Lamb. The species *P. banksiana* was often distributed on the edges of these clusters. This is an indication of strong common signals within species and genus. Clustering was also observed in the genus *Picea*; *T. occidentalis* had no specific locations within the reduced spaces.

The RDA indicated that the strongest climate influence was from the summer season (Fig. 2). Optimal tree growth and assimilation of carbohydrates for the next year's growth occurs if soil moisture is sufficient to maintain foliage water potential and minimize vapor pressure deficits. Of the total 43 significant monthly variables, 24 were related to June, July, or August from either the year prior $t - 1$ or current year t to ring formation. The July t CDC demonstrated a strong "negative" association with radial growth in five of six regions. In general, the genus *Pinus* (particularly *P. resinosa* and *P. strobus*) presented the strongest correlation with the July CDC (Fig. 2). August $t - 1$ temperature was a dominant variable in all six regions, and July $t - 1$, November $t - 1$, and April t temperatures were in three, three, and five regions, respectively. August $t - 1$ temperature more often pointed in the direction opposite to *Picea mariana* (Mill) B.S.P. and *P. banksiana.* Despite the absence of a relationship between the CDC and radial growth in the SL region, the combined effects of July $t - 1$ and August $t - 1$ mean temperatures suggested a negative effect of warm summer temperature on the next year's growth.

b. Reconstruction model performance

In all regions but SL, the mean July CDC was reconstructed as a proxy for summer drought. Because it is calculated on a daily weather cumulative scale, the mean July CDC gathers information over a season approximating May–July. The SL models did not allow accurate reconstruction of the CDC. Therefore, the mean July–August temperature was reconstructed as a proxy for midsummer temperature in the SL region. Despite the absence of a drought signal, the SL reconstruction provides valuable information on past climate variability, notably on the occurrence of midsummer warm spells and persistent ridging. Hereafter, the SL reconstruction is more often referred to as a "drought" reconstruction for consistency throughout the paper.

Figure 3 presents the regional model performance RE for the drought reconstructions plotted against the time period for which a multiple linear regression model was used. The best model obtained was the BP reconstruction with RE exceeding 0.30 for a reconstructed period reaching the early 1700s. The LS, LN, and APw reconstructions also showed good reconstruction skills for their whole period. The LN and APw reconstructions, however, demonstrated lower model coefficient of determination, R^2. Finally, both APe and SL reconstructions showed a decline of the RE statistic with a decrease in the number of predictors. The predictive skills of the submodels covering the nineteenth and twentieth centuries are high, and are acceptable for submodels covering the eighteenth century. Pearson correlation coefficients calculated between pairs of reconstruction submodels indicated that within any regions the submodels were sharing very strong common variance (Table 2): 75% of all coefficients were greater than 0.70.

c. Spatial and temporal patterns of drought variability

The regional drought reconstructions and their smoothed curves are shown in Fig. 4. Based on standard

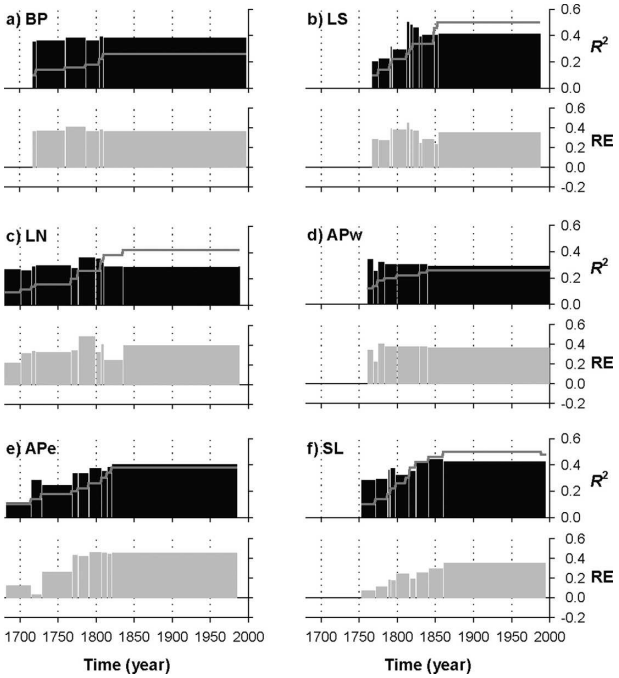

FIG. 3. Transfer function model R^2 for the calibration period 1919–84 (black bars) and the corresponding RE statistics (gray bars) for the verification period of 1919–40, plotted against the time period for which a given calibration model was used (1941–84). The R^2 is the fraction of the variance in instrumental data explained by the regression; the RE provides a sensitive measure of reconstruction reliability. Whenever RE is greater than zero the reconstruction is considered as being a better estimation of climate than the calibration period mean. The gray lines show the temporal developments of the number of chronologies used for the regional climate reconstructions (multiply the *y* scale by 50). Transitions from one submodel to another are delineated with vertical lines.

deviations of smoothed reconstructions >1.0 for at least four consecutive years, persisting dry events marked the BP region during 1735–43, 1838–43, 1887–92, 1936–40, and 1958–63. In the LS region, dry events marked 1791–95, 1838–42, 1860–67, 1908–11, 1932–37, and 1973–1983. In the APw and LN regions, dry events marked 1696–1700 (in LN), 1736–1744 (in LN), 1787–96, 1806–10, 1836–41 (in APw), 1888–92 (in APw), 1905–11, 1918–22, 1934–38, and 1991–95. In the APe region, dry events marked 1734–38, 1748–54, 1789–92, 1819–22, 1837–49, and 1917–22. Warm spells occurred in the SL region during 1791–96, 1876–82, 1909–16, and 1971–78. Finally, the 1718–1840 period was marked by a significant positive correlation between the western (BP) and eastern (APe) regions [$r = 0.24$; 95% bootstrap confidence interval (0.09; 0.39)], contrasting with the absence of correlation from 1841 to 1984 ($r = -0.12$).

A nonrotated PCA of the six drought reconstructions was run on the period 1768–1984; the first and second component scores (PC1 and PC2, respectively) were projected on a time axis (Fig. 5). The relationship was extended to 1718 by running a second PCA on the BP, LN, and APe reconstructions on their common interval from 1718 to 1984. The component scores from this last PCA were highly correlated with the former ones ($r_{pc1} = 0.87$ and $r_{pc2} = 0.77$ for $n = 217$, where n is the sample size). The intent of this work was to focus on the west–east gradient, and thus succeeding PCs were not accounted for.

PC1 shared common variability with all six reconstructions; its center was located over Lake Nipigon and the western Abitibi Plains (Fig. 5a). The component showed strong interdecadal drought variability in the 1770–1845 and 1905–1940 intervals. Wavelet analysis (Fig. 6a) effectively indicated the presence of high variance in the 17–32-yr band (accounts for 20.3% of the variance). The spectrum also showed high variance in the 9–16-yr band in the early 1800s and early 1900s (Fig. 6a). Starting in the 1940s, variance in this band weakened, suggesting a change in the pattern of drought variability during recent decades.

The PCA orthogonality constraint in space generally dictates the second PC to be a domain-wide dipole (e.g., about half the dataset being inversely correlated with the component loading). PC2 was effectively associated with a dipole between the western and eastern regions and thus was referred to as a meridional component (Fig. 5b). Positive PC2 scores indicated drier conditions in the BP–LS regions and lower drought severity in the APe–SL regions, and vice versa. PC2 (Fig. 5b) suggested that the twentieth century was marked by an increase in the magnitude of the meridional component, particularly of its decadal mode. Interdecadal variability has also occurred during the periods of 1718–50 and ~1830–70. Wavelet analysis (Fig. 6b) further indicated a period of increased variance in the 9–16-yr band during the late-twentieth century. Variance was also greater in the 17–32-yr band. The dynamics between PC1 and PC2 and the atmosphere are analyzed in the subsection that follows.

d. Tropospheric circulation

Prior to investigating the composites, tests were conducted to validate the use of the 500-hPa geopotential heights against PC1 and PC2. (Refer to appendix C for a description of the climatology.) Correlation maps with 500-hPa geopotential heights (not shown) indicated that variability in PC1 was associated with a north and south dipole, with one cell at 57°N, 95°W and another at 35°N, 90°W. In contrast, the second PC was associated with an east and west dipole, with one cell at 50°N, 115°W and the other at 50°N, 50°W. The zonal

TABLE 2. Relationships among reconstruction submodels per climatic regions. The values are Pearson correlation coefficients calculated between submodels using the interval of 1870–1984. The labels in italic indicate the number of chronologies used in the submodels. Refer to Fig. 3 for identification of intervals covered by the submodels.

	Pearson correlation coefficents										
BP	*5*	*6*	*8*	*10*	*11*	*13*					
5	1.00										
6	0.95	1.00									
8	0.91	0.95	1.00								
10	0.87	0.91	0.88	1.00							
11	0.86	0.89	0.87	0.98	1.00						
13	0.84	0.84	0.82	0.87	0.88	1.00					
LN	*5*	*6*	*7*	*8*	*10*	*13*	*15*	*17*	*19*	*21*	*24*
5	1.00										
6	0.96	1.00									
7	0.88	0.92	1.00								
8	0.84	0.83	0.96	1.00							
10	0.85	0.91	0.87	0.84	1.00						
13	0.83	0.83	0.75	0.74	0.87	1.00					
15	0.82	0.79	0.79	0.82	0.80	0.93	1.00				
17	0.82	0.81	0.85	0.89	0.84	0.87	0.96	1.00			
19	0.84	0.80	0.76	0.78	0.83	0.80	0.78	0.80	1.00		
21	0.79	0.77	0.72	0.73	0.81	0.80	0.77	0.78	0.99	1.00	
24*	0.78	0.75	0.69	0.70	0.80	0.79	0.75	0.77	0.98	0.99	1.00
APe	*5*	*7*	*9*	*10*	*11*	*13*	*15*	*17*	*19*	*20*	
5	1.00										
7	0.62	1.00									
9	0.66	0.84	1.00								
10	0.74	0.68	0.76	1.00							
11	0.75	0.55	0.64	0.95	1.00						
13	0.50	0.46	0.56	0.82	0.87	1.00					
15	0.51	0.48	0.57	0.83	0.87	1.00	1.00				
17	0.50	0.56	0.65	0.88	0.85	0.96	0.97	1.00			
19	0.49	0.56	0.66	0.87	0.85	0.95	0.96	1.00	1.00		
20*	0.39	0.61	0.64	0.78	0.72	0.75	0.76	0.83	0.85	1.00	
LS	*5*	*7*	*9*	*11*	*13*	*15*	*17*	*19*	*21*	*23*	*25*
5	1.00										
7	0.98	1.00									
9	0.78	0.82	1.00								
11	0.85	0.90	0.91	1.00							
13	0.57	0.64	0.66	0.67	1.00						
15	0.52	0.59	0.66	0.69	0.83	1.00					
17	0.53	0.59	0.57	0.64	0.83	0.97	1.00				
19	0.60	0.66	0.63	0.69	0.74	0.92	0.96	1.00			
21	0.56	0.61	0.60	0.66	0.71	0.89	0.94	0.98	1.00		
23	0.54	0.59	0.59	0.65	0.68	0.87	0.91	0.97	0.99	1.00	
25	0.55	0.60	0.58	0.68	0.67	0.86	0.90	0.94	0.96	0.97	1.00
APw	*6*	*7*	*9*	*10*	*11*	*12*	*13*				
6	1.00										
7	0.69	1.00									
9	0.66	0.73	1.00								
10	0.64	0.72	0.98	1.00							
11	0.64	0.71	0.97	1.00	1.00						
12	0.65	0.72	0.98	1.00	1.00	1.00					
13	0.64	0.71	0.98	0.99	0.99	1.00	1.00				

TABLE 2. *(Continued)*

	Pearson correlation coefficents								
SL	*5*	*7*	*9*	*11*	*13*	*19*	*21*	*23*	*25*
5	1.00								
7	0.93	1.00							
9	0.80	0.80	1.00						
11	0.85	0.79	0.87	1.00					
13	0.84	0.79	0.83	0.94	1.00				
19	0.85	0.89	0.79	0.87	0.89	1.00			
21	0.82	0.80	0.78	0.93	0.88	0.90	1.00		
23	0.81	0.83	0.77	0.85	0.82	0.90	0.94	1.00	
25	0.83	0.87	0.81	0.85	0.85	0.91	0.89	0.89	1.00

* These LN (1869–1987) and APe (1832–1984) submodels (RE = 0.17 and 0.26, respectively) were not included in the final reconstructions; their statistics were omitted from Fig. 3.

index (ZI) and the meridional index (MI) define these types of circulation (after Bonsal et al. 1999):

$$\mathrm{ZI} = \mathrm{Grad}(55^\circ \text{ to } 65^\circ\mathrm{N}) - \mathrm{Grad}(35^\circ \text{ to } 45^\circ\mathrm{N}) \quad (1)$$

and

$$\mathrm{MI} = Z(45^\circ \text{ to } 55^\circ\mathrm{N}, 115^\circ\mathrm{W}) - Z(45^\circ \text{ to } 55^\circ\mathrm{N}, 80^\circ\mathrm{W}), \quad (2)$$

where Z is the average 500-hPa value and Grad is the average 500-hPa gradient from 100° to 70°W (the approximate longitudinal extent of the study region). The ZI measures the characteristic of the west–east flow over the six regions, where +ZI defines a state with weak westerlies and strong meridional flow and −ZI is associated with strong westerlies and a weak meridional flow. The MI measures the meridionality of the flow, where +MI indicates an amplified western ridge and a deepened eastern trough and −MI indicates the reverse relation.

Time series of ZI and MI were correlated with their respective PC over the period of 1948–84 using the permuted Pearson coefficients. Results indicated that PC1 depicted significant responses to the ZI ($r = 0.46$, $p < 0.005$). Thus, it reflected variations in the strength of the westerly flow between the northern (55°–65°N) and southern (35°–45°N) regions. PC2 correlated well with the MI ($r = 0.45$, $p < 0.005$), indicating that it reflected variations in the western ridge and eastern trough. These results were comparable to calculations on PCs obtained from instrumental records over the interval of 1948–98 ($\mathrm{ZI}_{\mathrm{pc1}} = 0.41$, $\mathrm{MI}_{\mathrm{pc2}} = 0.43$).

Years of highest and lowest PC1 and PC2 scores were selected for the creation of 500-hPa geopotential height and vector wind anomaly composites (1948–84 period). A two-sample permutation test indicated a significant difference in means among samples of ZI indices at the time of the five highest and five lowest PC1 scores ($p = 0.016$). Similarly, a significant difference in means was observed among MI samples of the highest and lowest PC2 scores ($p = 0.009$). These two tests validated the use of the composite maps for exploration of the midtropospheric circulation variability associated with PC1 and PC2.

The 5 yr of positive PC1 (dry years; Fig. 7a) were associated, on average, with intensified ridging over the western Hudson Bay, lower-level divergence, and subsidence over much of the boreal forest (giving rise to drier conditions particularly in LN, APw, and APe regions). A meridional component gave rise to northeasterly winds in eastern Canada and southerly winds in the Great Plains. The 5 yr of −PC1 (Fig. 7b) were associated with lower heights over boreal Canada. As opposed to positive PC1 scores, −PC1 scores were associated with stronger midtropospheric westerlies and an amplified jet stream at 45°N and 70°–110°W. During years of low drought severity, moisture-bearing systems from the North Pacific Ocean were free to move across the continent. At 60°N the situation was the opposite, with the near absence of mid- and high zonal tropospheric winds (in absolute chart-reduced westerlies, not shown).

PC2 was, on average, associated with an oscillation in the position and direction of the jet stream and meridional flows from westward (positive PC2) to eastward (−PC2). Positive PC2 scores (Fig. 7c) were characterized by ridging over the Gulf of Alaska and Greenland and intensified troughing in eastern Canada. An anomalous anticyclonic flow over the Rocky Mountains, combined with the cyclonic flow above Ontario, gave rise to midtropospheric northwesterlies over central Canada and western Ontario. The persistence of the ridge induced subsidence of air over the eastern Boreal Plains, low precipitation, warming, and drying.

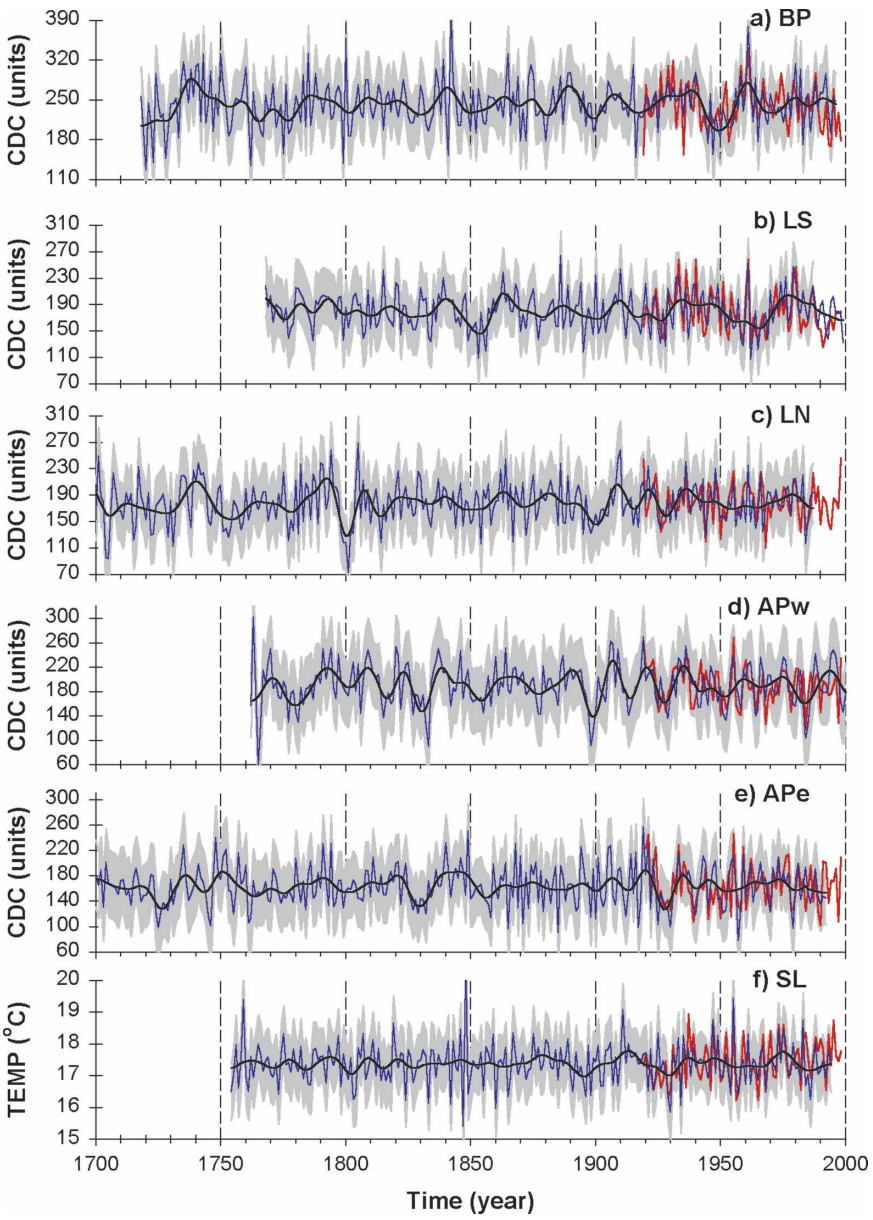

FIG. 4. Reconstructions of the mean July CDC (units) for the (a) BP, (b) LS, (c) LN, (d) APe, and (e) APw regions. The CDC scale ranges from soil saturation (zero) to extreme drought (>300). (f) Reconstruction of the SL mean July–August temperature (°C). Shaded area: error bars plotted against the time period for which a given calibration model was used. Red lines show instrumental 1913–98 records. Variance in the instrumental records was adjusted to correspond to reconstructions. Smoothed curves (black lines) were obtained from a polynomial fitting (order 6) across a moving 10-yr window within the data. These curves accounted for (a) 22.0%, (b) 22.8%, (c) 24.9%, (d) 35.1%, (e) 19.2%, and (f) 8.1% of the variance in the reconstructions.

In eastern Canada, the cyclonic activity drove midtropospheric southerlies along the U.S. east coast toward the Quebec interior. This flow allowed the advection of warm, moist, and unstable air from the subtropical North Atlantic basin into Quebec. The 5 yr of −PC2 (Fig. 7d) were associated with a weakening of the eastern trough, and a downstream convergence and subsidence zone near 70°W. The circulation was associated with southerlies in the Boreal Plains and western Boreal Shield that brought moisture-rich air from the coastal subtropical North Pacific. In eastern Quebec the anticyclonic flow drove an outflow of dry arctic air.

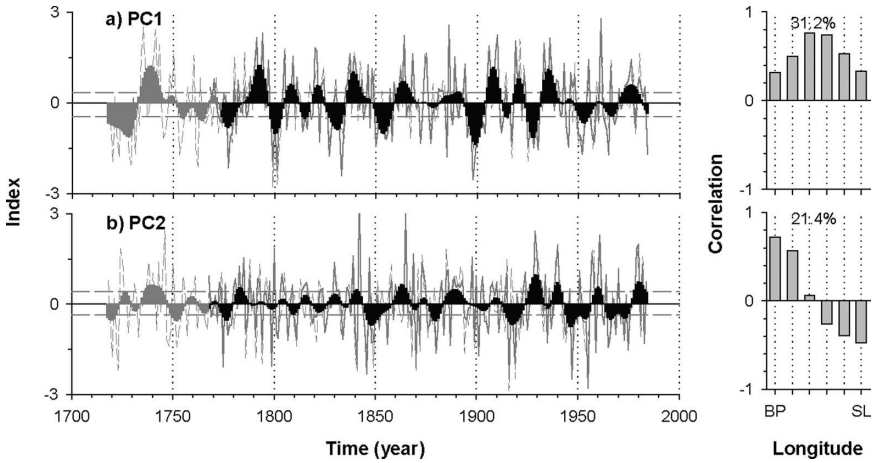

FIG. 5. (a) PC1 and (b) PC2 scores of the PCA (thin solid lines) illustrating the relationship among the six climate reconstructions over the common interval of 1768–1984. The vertical bar charts at right express the correlation coefficients between a PC score and a given climate reconstruction (BP for western and SL for eastern sectors); the percentage of expressed variance by the PC scores is indicated. Also projected are the PC scores covering the interval of 1718–67 (thin dashed lines) obtained from the BP, LN, and APe reconstructions. Smoothed PC scores are overlaid in black.

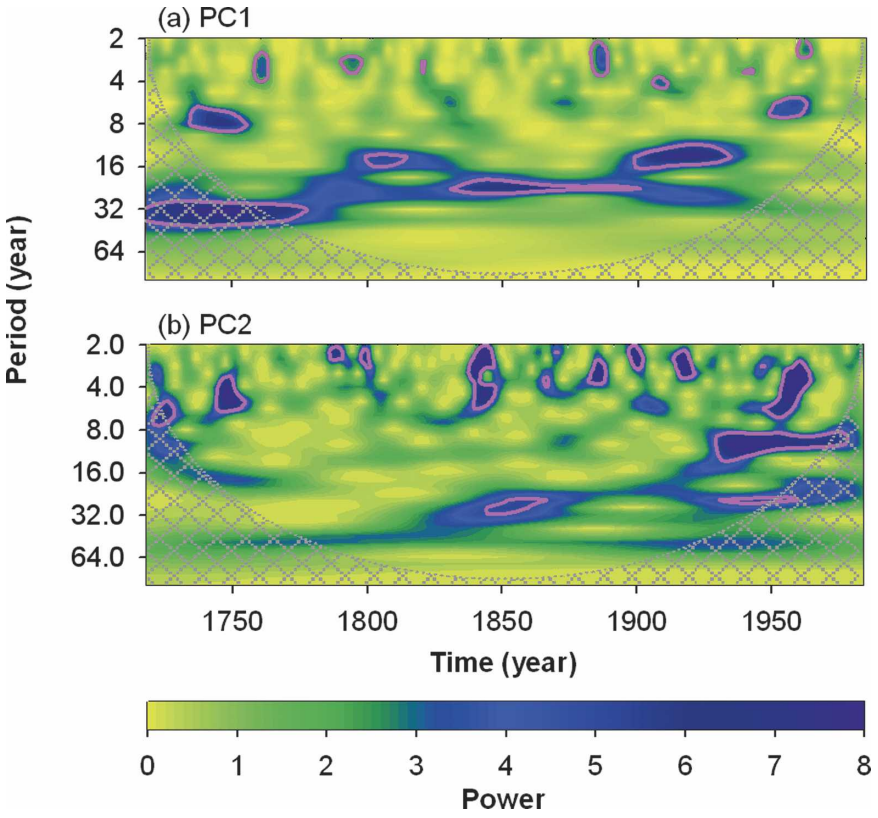

FIG. 6. Continuous wavelet transformation power spectrums of (a) PC1 and (b) PC2. The dark blue color indicates areas of large power; thick-red contour is the 5% significance level for red noise [AR(1) = 0.25 in (a) and AR(1) = 0.00 in (b)]. The cross-hatched regions on either end delineate the cone of influence where zero padding has reduced the variance. Note that for the period of 1718–67 the PCs were computed from only three climate reconstructions (BP, LN, and APe).

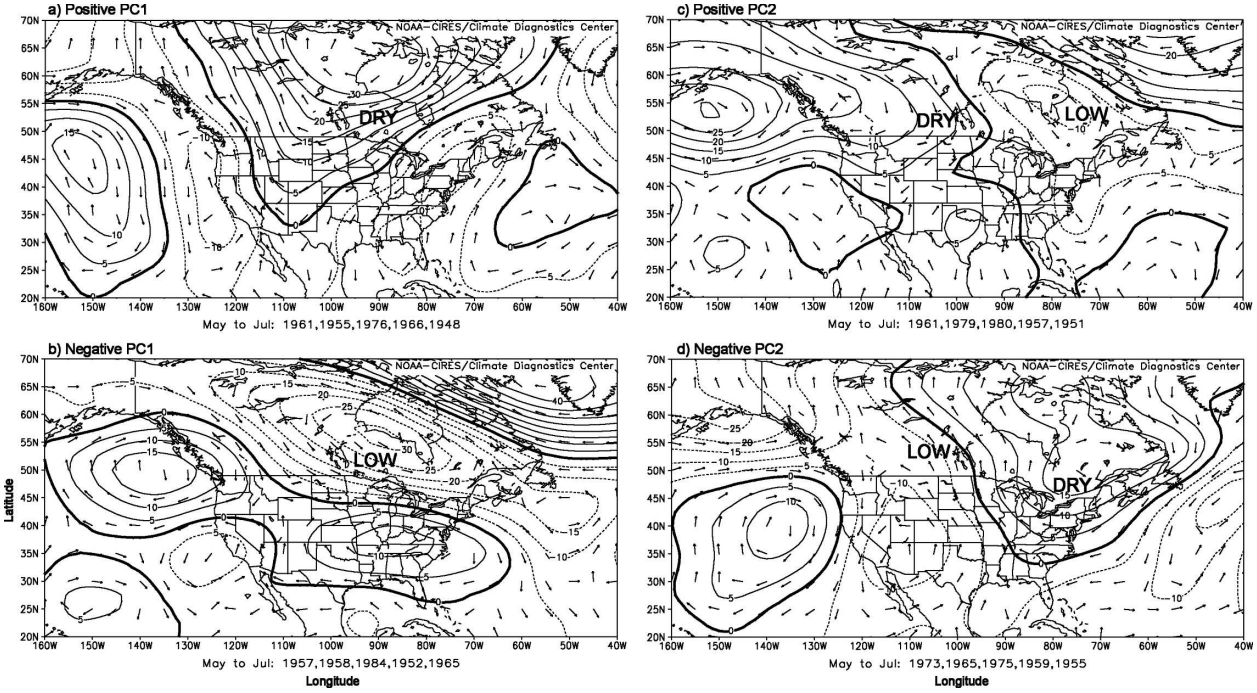

FIG. 7. May–July 500-hPa geopotential height anomaly composites (5-m contour intervals) for 5 yr of (a) highest PC1 scores, (b) lowest PC1 scores, (c) highest PC2 scores, and (d) lowest PC2 scores. Regions of anomalously low (LOW) and high (DRY) drought severities are indicated. Solid contours indicate positive anomalies; dashed contours indicate negative anomalies (zero interval is boldface). Directions of 500-hPa vector wind anomalies (arrows) are also shown. The anomalies were calculated from the mean of the reference period of 1968–96. Years used in the composites are listed below each map.

The PCs are additive, so any pattern from PC1 (either Fig. 7a or 7b) can be superimposed on any pattern from PC2 (Fig. 7c or 7d). For instance, PC1 indicated that 1955 was generally dry over the LS, LN, and APw regions. PC2 indicated that it was drier in APe than in BP. Climatologically, this suggested that the circulation in 1955 featured a strong anticyclone (i.e., Fig. 7a), but with a center located northeast of Ontario.

e. Sea surface temperatures

The connection between the west–east meridional component (PC2) and global ERSST is presented in Fig. 8. Analyses conducted on PC1 show no significant correlation with the mean May–July SST, and thus are not presented. A PC2 correlation chart (not shown) indicated a significant positive correlation ($p < 0.05$) with SST along the eastern North Pacific coast and into the Tropics. A center of significant negative correlation was also observed in the interior North Pacific, roughly at 160°W and 30°N. The spatial structure of the variability was very similar to that of the Southern Oscillation (Ropelewski and Jones 1987), but with greater amplitude at high latitudes and a reduced tropical expression. The Pacific pattern is the one commonly referred to as the Pacific decadal oscillation (PDO; Mantua et al. 1997; Zhang et al. 1997) or North Pacific pattern (Latif and Barnett 1996). A significant Pearson correlation between PC2 and the May–July ERSST PDO of Smith and Reynolds (2003; not shown) was obtained [$r = 0.25$ with 95% confidence interval (0.09; 0.39), period 1854–1984]. Analysis between the PDO and PC2 10–30-yr/cycle waveforms (not shown) further indicated a highly significant correlation in the interdecadal mode with $r = 0.72$ (0.64; 0.79). [Correlations were computed using a nonparametric stationary bootstrap that accounts for autocorrelation in the data (PearsonT software; Mudelsee 2003).]

A two-sample permutation test indicated a significant difference in means among samples of ERSST PDO indices at the time of the 10 highest and the 10 lowest PC2 scores ($p < 0.004$). Figure 8a indicated that positive PC2 were associated with higher SSTs along the western coast of North America. A center of positive anomalies not dissimilar to the typical El Niño signature, but with reduced expression, was also observed in the tropical Pacific, roughly at 150°W. Two centers of lower-than-normal SSTs were observed in the interior North Pacific near 37°N, 160°W, and in the western

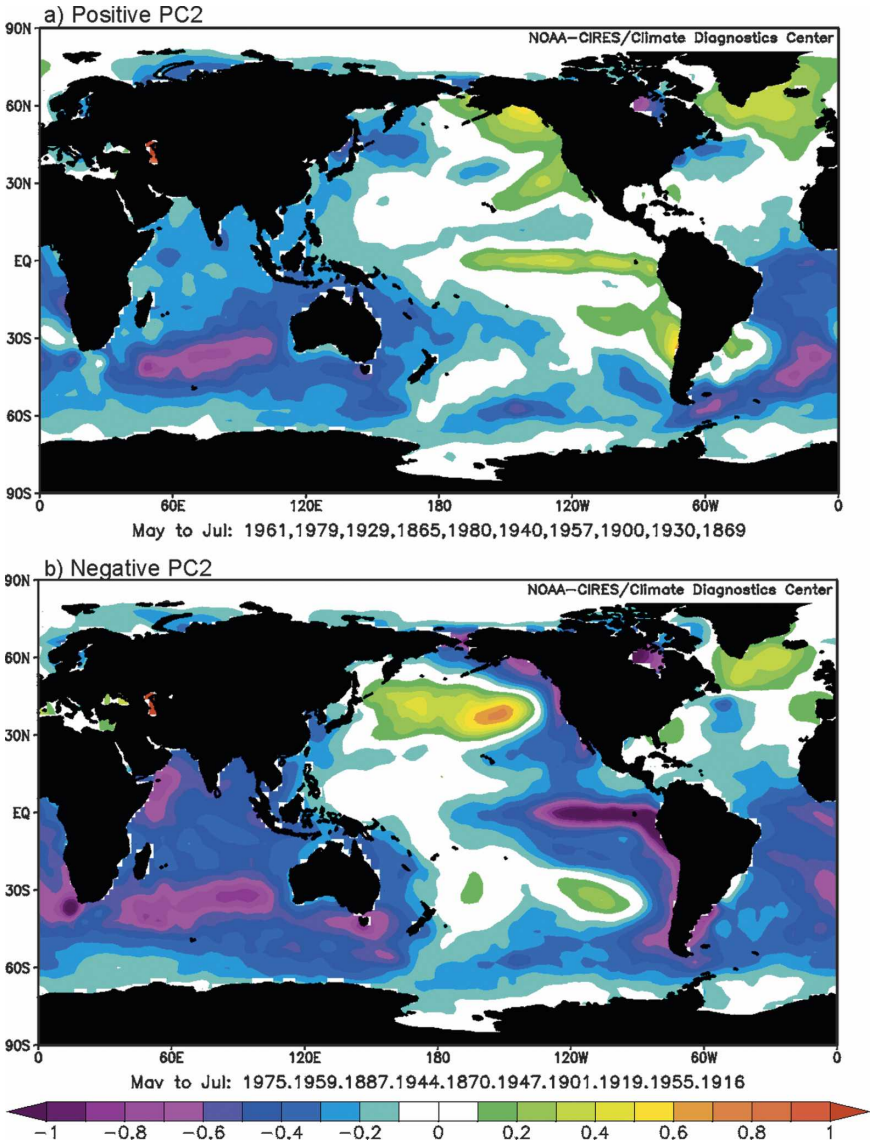

FIG. 8. May–July SST anomaly composites for 10 seasons of (a) highest PC2 scores and (b) lowest PC2 scores over the interval of 1854–1984. The anomalies were calculated from the mean of the reference period of 1971–2000. Years used in the composites are listed below each map.

North Pacific near 45°N, 155°W (Fig. 8a). In the South Pacific, a similar pattern was observed, with warmer SSTs along the American coast.

During average PC2 scores (not shown), the interior North Pacific anomaly shifted in sign. Lower SST occurred in the tropical and east subtropical North Pacific and along the western coast of North America and South America. During negative PC2 scores (Fig. 8b), the center of anomalously positive SSTs in the interior North Pacific intensified. SSTs lowered to reach an average of ~1.5°C below normal in the eastern tropical and subtropical North Pacific (the typical La Niña signature) and ~0.7°C below normal along the western coast of Alaska. In the South Pacific, a similar pattern was observed, with warmer SSTs in the interior and cooler SSTs along the South American coast.

f. Frequency of composite types

Histograms showing the frequency per decades of positive and negative PC score departures were created (Fig. 9). The PC scores were classified as being either part of the upper 33.3% percentiles (positive PC departures), lower 33.3% percentiles (negative PC departures), or in between (residual PC departures). The

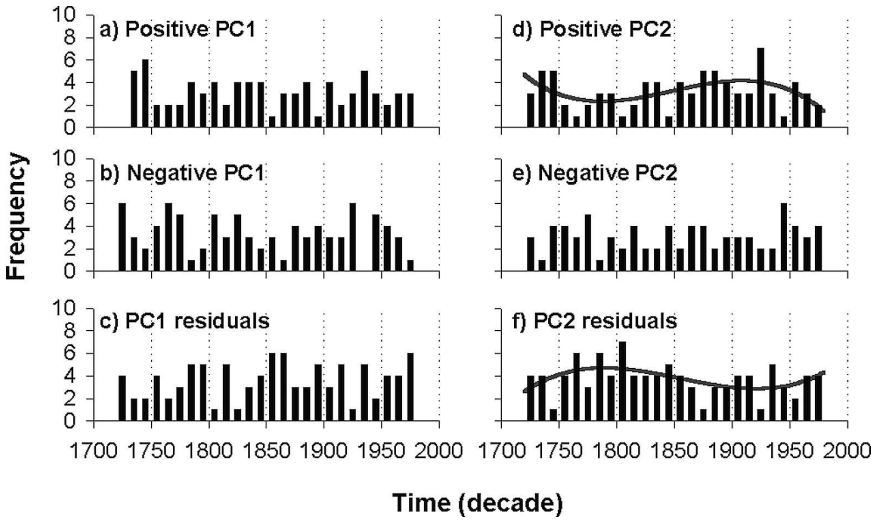

FIG. 9. Histograms showing the frequency per decade of PC1 and PC2 positive and negative departures exceeding the higher and lower 33.3% percentiles from the long-term mean of the reference period of 1718–1984. The frequency per decade of nondeparture years (PC residuals) is also shown. Third-order polynomial regression lines accounting for (d) 22.6% and (f) 20.4% are shown. PCs were obtained from the analysis of the BP, LN, and APe reconstructions.

33.3% percentile threshold was arbitrarily chosen and results were consistent with the 20.0% and 40.0% thresholds.

The temporal distribution of the PC2 scores suggested a period of less frequent positive PC2 from 1751 to 1850, with the exception of the intervals of 1781–1800 and 1821–40. The 1751–1850 interval contrasted with periods of frequent positive PC2 from 1721–50 and 1851–1940 (Fig. 9d). From 1751 to 1850, positive PC2 occurred at an average rate of 2.3 yr decade^{-1}, whereas from 1851 to 1940 the average was 4.1 yr decade^{-1}. This change in the frequency of occurrences of positive PC2 in 1850 was tested significant using a two-sample permutation test ($p = 0.006$). A significant change toward a reduced frequency in the residuals of PC2 (Fig. 9f) from the former period to the later was also detected ($p = 0.018$). No significant change was detected in the frequency of PC1 and negative PC2 departures.

Climatologically, this change in the frequency of PC2 scores suggested a period of greater zonality from 1751 to 1850 across the eastern Boreal Plains and Boreal Shield during the summertime. It implied that less frequent ridging and air subsidence marked 1751–1850 over the eastern Boreal Plains, while in the eastern Boreal Shield it meant a weaker trough and less frequent advection of humid air masses from the subtropical North Atlantic. The midtropospheric pattern associated with Fig. 7c and the SST pattern associated with Fig. 8a (cooler SST in the interior North Pacific and warmer ones along the American North Pacific coast and in the Tropics) were likely less frequent from 1751 to 1850. The atmospheric transition at ~1850 is further investigated in the next subsection.

g. *Validation of spatiotemporal variability*

The temporal stability of the shared variance among regions was evaluated by conducting a PCA on a rectangular matrix of 90 multicentury tree-ring residual chronologies, sharing the common period of 1781–1980, and distributed across a rectangular grid covering from 41° to 61°N and from 101° to 61°W (Fig. 10) (e.g., Fritts et al. 1991; Bradley 1999; Gajewski and Atkinson 2003; Tardif et al. 2003). The rectangular matrix was created by nesting 58 chronologies located within our six climate regions into a grid composed of 32 chronologies from surrounding areas (Fig. 1; appendix A). All measurement series were processed as described in section 2b. The 1781–1980 period was chosen to maximize the length of the period of analysis, the number of chronologies in each region, and the subsignal strength. The shared variance was analyzed by constructing four sequential maps, each one representing the chronology loadings on a principal component for a given period of 100 yr. Though species were unequally distributed in the area of study, the approach was justified by the persistence of the relationship between radial growth and climate in the six regions.

The analysis of the interval of 1781–1880 (Fig. 10a)

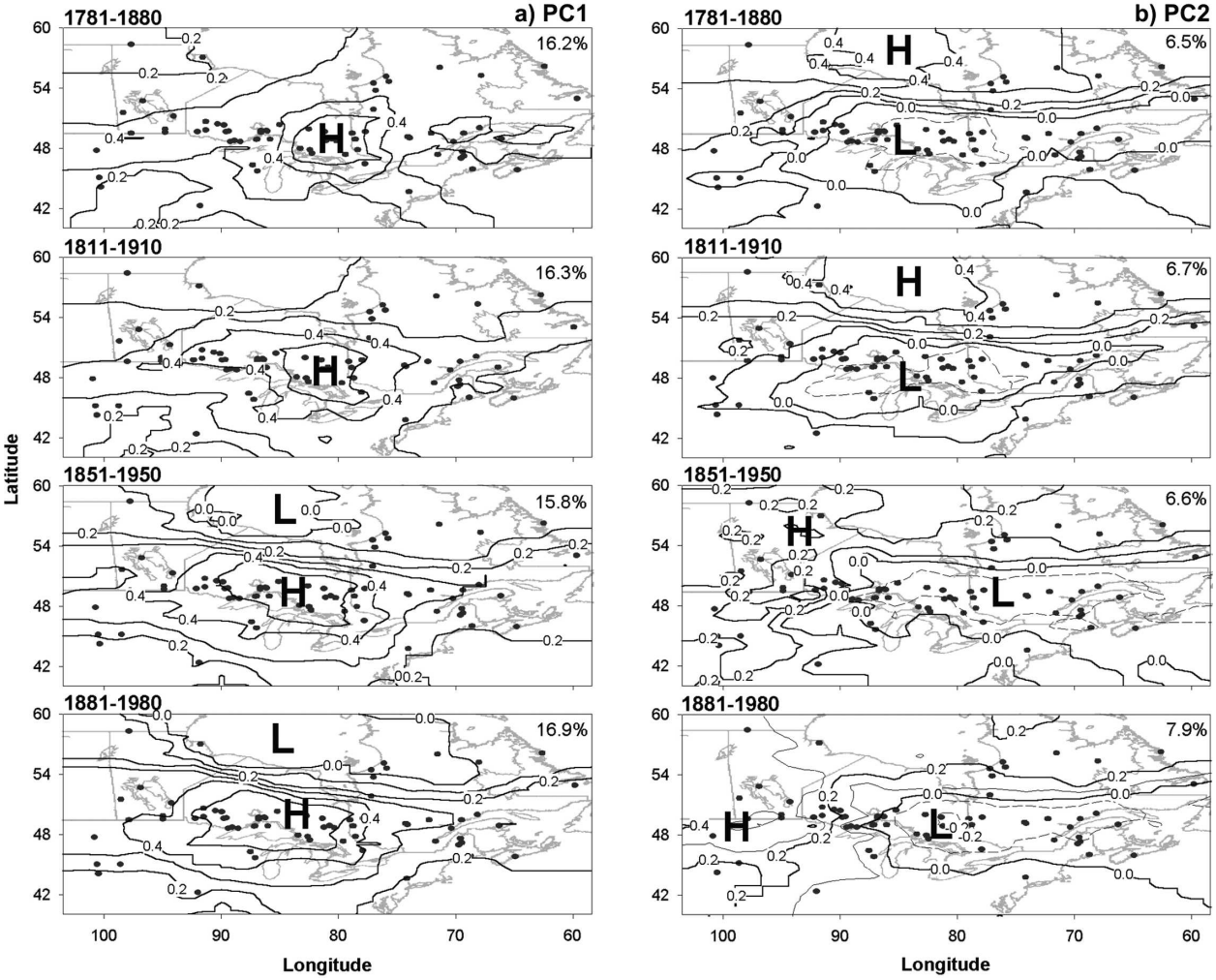

FIG. 10. Spatial correlation fields of (a) PC1 and (b) PC2 of the 90 tree-ring chronologies for different 100-yr time periods. The respective eigenvalues are shown (%). Centers of positive (H) and negative (L) correlation are indicated. The total sum of the squares of the data matrix for each time period is 262.1, 236.2, 209.6, and 218.6, respectively. PCA was conducted using the correlation matrix.

indicated that in the earliest period, chronologies from all sectors shared common variance. After 1851, a breakup of the common signal was observed with the weakening of the correlation coefficients between PC1 and chronologies from northern Canada and Quebec. This transition from a domain-wide pattern to a dipole likely reflects a shift in midtropospheric wind flow between the north and south. The percentage of explained variance has not changed substantially from the first interval to the last.

In the earliest interval, PC2 (Fig. 10b) was characterized by a north–south dipole with the axis (zero line) passing through approximately 55°N. The dipole was weak on its negative center (average correlation >-0.20) and strong on its positive one (average correlation <0.45). In the interval after 1851, the orientation of the dipole shifted toward a west–east direction with the axis passing through approximately 90°W, that is, just west of Lac Seul. This is the current location of the average summer position of the axis dividing the western ridge from the eastern trough (refer to Figs. 7c–d).

4. Discussion

a. Atmospheric circulation

The presented analyses provide new information on the year-to-year and decade-to-decade variability of summer drought severity along the southern limit of the Canadian boreal forest. Results suggest that the area covering the eastern Boreal Plains to the eastern Boreal Shield is under the influence of two components of large-scale atmospheric circulation. The zonal compo-

nent (PC1) is associated with a circulation of cool and moist westerlies over the central area of the Boreal Shield during years of low drought severity, and a circulation of dry and cold northerlies during years of high drought severity. The analysis of the component's spectra showed high variance in the 17–32-yr band over most of the reconstructed period. The analysis revealed no major changes in either its magnitude at ~1850, or in its spectra. Changes were, however, noted in other periods, with strong variance in high-frequency bands around 1800 and 1900 and low variance in the late-twentieth century. Despite the absence of changes in the component in ~1850, analysis of the spatiotemporal variability in radial growth over the eastern half of Canada and the United States suggested that the expression of the zonal pattern has changed between the northern and the southern areas of the Boreal Shield. This shift would corroborate with the reported contraction of the Aleutian and Icelandic lows in 1850 (Guiot 1985; Gajewski and Atkinson 2003).

The meridional component reflects regional drought variability in the west–east dimension. This variability occurs as a response to the blocking of moisture-carrying systems upstream and advection of moisture air downstream of the long waves (Flannigan and Harrington 1988; Weber 1990; Knox and Lawford 1990; Bonsal et al. 1999; Skinner et al. 1999, 2002). An amplified western ridge is associated with a northerly displacement of the jet stream over western Canada and a southerly displacement in eastern Canada. This configuration favors northerly winds, air subsidence, and increasing drought severity in the eastern Boreal Plains. In the eastern Boreal Shield, this configuration favors cyclonic development, inflows of subtropical North Atlantic air, and lower drought severity. Spatiotemporal analyses conducted on the six reconstructions and the multicentury tree-ring chronologies suggested that the meridional component has gained in magnitude over the past 150 yr and particularly in the decadal scale of variability. This suggested that more intense longwave oscillations occurred during the past century over the Canadian boreal forest, contributing to a greater contrast in summer drought severity between the eastern Boreal Plains and eastern Boreal Shield. Analyses of year-to-year variability suggested that from ~1751–1850, amplifications of the western ridge and eastern trough were likely infrequent relative to ~1851–1940 (Fig. 9c). This meant reduced frequency in the occurrence of air subsidence in the eastern Boreal Plains and airmass advection in the eastern Boreal Shield during the former interval.

Skinner et al. (1999) addressed the effect of atmospheric circulation shifts on the area burned across Canada. A transition toward a higher frequency of ridging (troughing) over western (eastern) Canada after 1974 contributed to significant increases in the area burned, especially in the northwest and central regions (1975–95 versus 1953–74). Analyses by Girardin et al. (2004b) effectively showed significant correlations between seasonal area burned across the six regions during the period of 1959–98 and the instrumental zonal PC1 and meridional PC2. However, despite the fact that the season covered by the reconstructions may be a good proxy for fire weather conditions at the time of the greatest area burned, it may underestimate or omit variability and temporal changes in conditions leading to spring and late-summer fires. In Canada, 78% of the area burned from 1959 to 1998 occurred in June and July, while 8% occurred during May and 13% during August (Stocks et al. 2003).

The temporal changes reported are in the year-to-year and decade-to-decade scales of variability. Little attention was given to the reconstruction of low-frequency variations. In the past year or so discussions have taken place regarding various methods applied to standardize tree-ring data (e.g., Esper et al. 2002). The debate is focused on differencing the long-term climate signal from the long-term tree growth signal. For instance, the different approaches of tree-ring data standardization appear to most substantially account for the differing low-frequency trends in the reconstructed Northern Hemisphere temperature (Esper et al. 2002). The use of nonconservative detrending may however be increasingly important in tree-ring data showing noise resulting from stand disturbances (herbivory and post–forest fire growth releases). But most importantly, the period covered by most samples collected in the boreal forest is insufficiently long to allow for robust reconstruction of low-frequency variations. The contribution of other types of proxies could be valuable in attempting to reconstruct low-frequency changes that may superimpose on those reported in this work.

b. North Pacific air–sea interactions

It is now commonly accepted that the atmospheric response to SST anomalies in the equatorial Pacific determines ocean conditions over the remainder of the global ocean (Yang and Zhang 2003; Kumar and Hoerling 2003; Lau et al. 2004; Shabbar and Skinner 2004). Tropical SSTs, with the contribution of stochastic feedback from the atmosphere, generate the North Pacific SST anomalies (Schneider et al. 2002; Newman et al. 2003; Wu and Liu 2003). Wu and Liu (2003) indicated that anomalies in the central and eastern North Pacific Ocean, well simulated by global ocean–atmosphere models, could be obtained from anomalous Ekman

transport and surface heat flux. Lau et al. (2004) suggested a mechanism in which air–sea interactions amplify North Pacific anomalies and sustain them through feedback processes, involving the interplay of surface fluxes, atmospheric mean circulation and transient eddies, and radiation effects of stratocumulus cloud decks.

Several paleoclimate studies suggested important changes in the North Pacific climate over the past three centuries (Luckman et al. 1997; Stahle et al. 1998; D'Arrigo et al. 2001; Evans et al. 2002; Finney et al. 2000; Gedalof et al. 2002; Wilson and Luckman 2003). The significant association observed between the meridional component and tropical and North Pacific SSTs indicated that spatiotemporal drought variability over the eastern half of Canada has been under the influence of this coupling for a period covering at least 150 yr. Because of the relationship between Pacific SSTs and atmospheric circulation, the combined information from these studies could support the observation of a weakened western ridge and eastern trough from ~1760 to 1840. Investigation of prominent aquatic population declines in the Gulf of Alaska by Finney et al. (2000) suggested the prevalence of cooler water along the coast from approximately 1750 to 1850. A prolonged period of cooler Pacific and western coast air temperature during the preindustrial period was also reported by Luckman et al. (1997), D'Arrigo et al. (2001), Evans et al. (2002), and Wilson and Luckman (2003). Reconstruction of the Southern Oscillation index (SOI) by Stahle et al. (1998) showed a statistically significant increase in the SOI interannual variability during the mid-ninetieth century. Though there may be a teleconnection, the meridional component developed here is not optimized to capture the maximum atmospheric circulation variability associated with the Pacific, and thus it should not be interpreted as a proxy for past SST variability.

This study may be complementary to recent work by Jacobeit et al. (2003) in which July dynamical modes of atmospheric circulation in Europe were reconstructed. The authors also observed a period dominated by a westerly flow from about 1750 toward the end of the nineteenth century. Thereafter, a steady increase of a meridional component followed, which was associated with increasing anticyclonic activity over the eastern North Atlantic and the European continent. While it is difficult to link European and Canadian climate variability, the combined information from this study and that of Jacobeit et al. (2003) suggests that the circulation transition at about 1850 from zonal to meridional flows could be part of a global-scale phenomenon. In the context of global ocean teleconnections, it is suggested that North Pacific and North Atlantic SST patterns may be connected through an extratropical climate mode, linking SST variability in the North Pacific and the North Atlantic via an atmospheric bridge across North America (Lau et al. 2004).

c. Concluding remarks

This work constitutes an important step in the development of climate change adaptation strategies in the Canadian boreal forest sector. Paleoclimate information can improve our understanding of how the atmosphere–ocean and land climate systems have evolved over the past centuries, and provide a baseline to anticipate future vegetation response to climate variability and change across Canada. The results suggest that broad-scale atmospheric circulations are important in meteorological conditions like drought. Fire is related to weather, and more specifically drought, so it is likely that uncovered atmospheric patterns have also influenced forest fires and vegetation dynamics over the past centuries. In the light of the present findings, it is pertinent to believe that the decrease in the frequency of large areas burned around 1850 on the eastern Canadian Boreal Shield is because of the more frequent advection of air masses from the subtropical North Atlantic. The meridional circulation is however highly variable in the decadal scale, and this variability likely gave rise to several succeeding episodes of severe and prolonged midtropospheric circulation blocking during the past 80 yr or so.

Acknowledgments. We acknowledge the Sustainable Forest Management Network for funding this research and supporting M. P. Girardin. The author was also supported by doctoral scholarships from the Fonds Québécois de la Recherche sur la Nature et les Technologies and the Prairies Adaptation Research Collaborative. The field and laboratory work for the development of the Ontario chronologies could not have been done without the incredible support of Elizabeth Penner and Daniel Card. We thank Ontario Provincial Park for granting us permission to conduct this research in their parks. Thanks to Stan Vasiliauskas, Ed Iskra, Don Armit, Charlotte Bourdignon, and Dave New from the Ontario Ministry of Natural Resources and Timothy Lynham from the Canadian Forest Service for making our search of old trees in Ontario successful. We thank NOAA (NCEP–NCAR reanalysis project) and the Meteorological Service of Canada for their aid and contribution of climate data. We thank Kim Monson, Danny Blair, Malcom Cleaveland, and two anonymous reviewers for commenting on and editing the manuscript.

APPENDIX A

Sources of Tree-Ring Chronologies

TABLE A1. Sources of the tree-ring chronologies. Mean is mean length of measurement series; *N* is the sample depth of the tree-ring series; SSS is the subsample signal strength and is used to define the portion of the residual chronology (year *y* to present) with a strong common signal (Wigley et al. 1984); and Sens is mean sensitivity of the residual chronology, with NA for information not available.

	Species	Contributors*	Location	Lat (°N)	Lon (°W)	Period	Mean (yr)	*N*	SSS > 0.85 (yr)	Sens
Boreal Plains										
1	*Quercus macrocarpa*	Ss	Red River Alluvial Logs	49.20	97.10	1448–1999	98	92	1523	0.19
2	*Quercus macrocarpa*	Ss	Kildonan Park	49.56	97.06	1720–1999	137	44	1851	0.24
3	*Thuja occidentalis*	Tj	Middlebro	49.27	95.23	1802–2003	130	20	1875	0.16
4	*Thuja occidentalis*	Tj	Cedar Lake	53.00	99.16	1713–1999	117	77	1811	0.14
5	*Pinus resinosa*	Tj	Black Island	51.10	96.30	1709–2001	102	148	1724	0.15
6	*Larix laricina*	Tj	Duck Mountain Provincial Forest	51.60	101.00	1676–2002	99	89	1729	0.21
7	*Picea mariana wet*	Tj	Duck Mountain Provincial Forest	51.60	101.00	1758–2001	177	64	1795	0.13
8	*Picea mariana dry*	Tj	Duck Mountain Provincial Forest	51.60	101.00	1724–2000	156	19	1895	0.16
9	*Pinus banksiana*	Tj	Duck Mountain Provincial Forest	51.60	101.00	1717–2001	87	521	1757	0.15
10	*Picea glauca*	Tj	Duck Mountain Provincial Forest	51.60	101.00	1776–2001	129	81	1829	0.18
11	*Populus balsamea*	Tj	Duck Mountain Provincial Forest	51.60	101.00	1808–2001	106	47	1890	0.28
12	*Populus tremuloides*	Tj	Duck Mountain Provincial Forest	51.60	101.00	1806–2001	94	264	1888	0.25
13	*Betula papyrifera*	Tj	Duck Mountain Provincial Forest	51.60	101.00	1785–2001	102	114	1893	0.24
Lac Seul Upland and Lake of the Woods										
14	*Picea glauca*	Sf	Bruno Lake	51.37	95.50	1822–1988	126	24	1846	0.19
15	*Picea glauca*	Sf	High Stone Lake	50.24	91.27	1813–1988	130	25	1827	0.18
16	*Pinus resinosa*	Gm	Caliper Lake Provincial Park	49.05	93.92	1851–2001	134	17	1857	0.20
17	*Pinus resinosa*	Gm	Kenora	49.92	94.12	1792–2001	129	41	1828	0.16
18	*Pinus resinosa*	Gm	Sioux Lookout Provincial Park	49.42	94.05	1772–2001	134	44	1808	0.23
19	*Pinus strobus*	Gm	Longbow Lake	49.72	94.28	1789–2002	123	41	1844	0.21
20	*Pinus resinosa*	Gm	Longbow Lake	49.72	94.28	1830–2001	157	43	1836	0.23
21	*Pinus banksiana*	Gm	Highway 105	50.45	93.12	1815–2001	130	44	1818	0.19
22	*Pinus banksiana*	Gm	Lake Packwash Provincial Park	50.77	93.43	1852–2001	86	12	1872	0.21
23	*Pinus resinosa*	Gm	Lake Packwash Provincial Park	50.75	93.43	1744–2002	168	38	1823	0.20
24	*Pinus strobus*	Gm	Camping Lake	50.58	93.37	1827–2002	112	37	1857	0.17
25	*Thuja occidentalis*	Gm	Lac Seul south	50.27	92.28	1762–2002	110	42	1875	0.17
26	*Pinus resinosa*	Gm	Lac Seul south	50.32	92.28	1837–2001	132	40	1855	0.12
27	*Pinus resinosa*	Gm	Red Lake	51.08	93.82	1818–2001	155	41	1823	0.18
28	*Pinus banksiana*	Gm	Snail Lake	50.87	93.38	1847–2002	91	24	1898	0.17
29	*Pinus resinosa*	Gm	Stormy Lake	49.35	92.23	1791–2001	112	37	1812	0.14
30	*Pinus strobus*	Gm	Eagle Lake	49.77	93.33	1712–2002	126	40	1765	0.22
31	*Pinus resinosa*	Gm	Eagle Lake	49.78	93.33	1808–2001	146	39	1825	0.18
32	*Pinus strobus*	Gm	Sioux Lookout	50.07	91.92	1784–2002	112	40	1848	0.17
33	*Pinus resinosa*	Gm	Sioux Lookout	50.07	91.92	1766–2002	116	29	1807	0.18
34	*Pinus resinosa*	Gm	Sowden Lake	49.53	91.17	1640–2001	216	40	1738	0.15
35	*Pinus strobus*	Gm	Sowden Lake	49.53	91.17	1816–2002	110	39	1836	0.18
36	*Pinus strobus*	Gm	Turtle River Provincial Park	49.25	92.22	1810–2001	104	34	1834	0.15
37	*Pinus resinosa*	Gm	Lake Sandbar Provincial Park	49.45	91.55	1828–2000	100	35	1899	0.19
38	*Pinus strobus*	Gm	Lake Sandbar Provincial Park	49.45	91.55	1773–2002	104	54	1902	0.18
Lake Nipigon										
39	*Pinus resinosa*	Gl	Saganaga Lake	48.00	90.00	1719–1988	188	43	1780	0.23
40	*Pinus resinosa*	Sc	Ed Shave Lake	48.00	91.00	1700–1982**	162	38	1797	0.24
41	*Pinus resinosa*	Gl	Saganaga Lake	48.13	90.54	1644–1988	201	51	1693	0.26
42	*Betula papyrifera*	Gm	Rainbow Fall Provincial Park	48.50	87.38	1766–2001	143	48	1783	0.33
43	*Picea glauca*	Gm	Rainbow Fall Provincial Park	48.50	87.38	1788–2001	122	58	1813	0.19
44	*Thuja occidentalis*	Gm	Rainbow Fall Provincial Park	48.50	87.38	1774–2001	141	42	1825	0.15
45	*Pinus strobus*	Gm	Nipigon	49.23	88.17	1833–2002	98	47	1861	0.17
46	*Pinus banksiana*	Gm	Lake Nipigon Provincial Park	49.45	88.12	1866–2001	101	30	1875	0.16
47	*Pinus banksiana*	Gm	Shakespeare Island	49.62	88.08	1864–2002	83	62	1871	0.14
48	*Thuja occidentalis*	Gm	Beardmore campground	49.53	87.82	1734–2001	141	56	1819	0.15
49	*Thuja occidentalis*	Gm	Beardmore marina	49.63	88.08	1677–2001	154	69	1814	0.12

TABLE A1. *(Continued)*

	Species	Contrib-utors*	Location	Lat (°N)	Lon (°W)	Period	Mean (yr)	*N*	SSS > 0.85 (yr)	Sens
50	*Picea glauca*	Gm	MacLeod Provincial Park	49.68	87.90	1804–2000	140	50	1835	0.15
51	*Thuja occidentalis*	Gm	MacLeod Provincial Park	49.68	87.90	1790–2001	116	43	1859	0.14
52	*Thuja occidentalis*	Gm	Upper Twin Lake	50.15	86.55	1772–2001	124	32	1842	0.17
53	*Picea mariana*	Gm	Upper Twin Lake	50.15	86.55	1797–2002	150	39	1812	0.13
54	*Pinus banksiana*	Gm	Longlac	49.67	86.22	1847–2001	105	34	1864	0.21
55	*Picea mariana*	Gm	Sleeping Giant Provincial Park	48.37	88.82	1676–2001	132	30	1785	0.16
56	*Pinus banksiana*	Gm	Sleeping Giant Provincial Park	48.47	88.73	1817–2001	101	35	1826	0.18
57	*Thuja occidentalis*	Gm	Sleeping Giant Provincial Park	48.45	88.73	1713–2001	140	33	1828	0.13
58	*Pinus resinosa*	Gm	Sleeping Giant Provincial Park	48.45	88.73	1805–2001	159	41	1817	0.19
59	*Pinus strobus*	Gm	Sleeping Giant Provincial Park	48.45	88.73	1805–2001	116	42	1840	0.16
60	*Pinus strobus*	Gm	Sleeping Giant Provincial Park	48.43	88.75	1807–2001	145	53	1814	0.17
61	*Thuja occidentalis*	Gm	Sleeping Giant Provincial Park	48.37	88.82	1662–2001	162	55	1746	0.12
62	*Thuja occidentalis*	Gm	Sleeping Giant Provincial Park	48.32	88.87	1665–2001	137	68	1824	0.14
Abitibi Plains west										
63	*Thuja occidentalis*	Gm	Fushimi Lake Provincial Park	49.83	83.92	1765–2002	154	34	1815	0.14
64	*Picea mariana*	Gm	René-Brunelle Provincial Park	49.42	82.13	1721–2002	148	50	1790	0.13
65	*Pinus strobus*	Gm	Geiki Lake	48.18	81.08	1709–2002	96	41	1876	0.17
66	*Pinus resinosa*	Gm	Blue Lake	48.58	81.72	1606–2002	223	46	1772	0.19
67	*Pinus banksiana*	Gm	Blue Lake	48.58	81.72	1760–2002	156	55	1772	0.17
68	*Pinus banksiana*	Gm	Foliyet	48.23	82.00	1769–2002	113	30	1819	0.17
69	*Pinus resinosa*	Gm	Ivanhoe Lake Provincial Park	48.15	82.50	1828–2002	126	38	1848	0.17
70	*Thuja occidentalis*	Gm	Missinaibi Provincial Park	48.27	83.40	1798–2002	128	43	1842	0.17
71	*Pinus resinosa*	Gm	Highway 556	46.87	83.45	1837–2002	144	33	1848	0.14
72	*Thuja occidentalis*	Gm	Highway 556	46.88	83.43	1760–2002	130	44	1827	0.17
73	*Pinus strobus*	Gm	Ranger Lake	47.02	83.88	1760–2002	99	40	1823	0.22
74	*Pinus strobus*	Gm	Montreal River	47.22	84.63	1779–2002	117	33	1880	0.20
75	*Pinus resinosa*	Gm	Montreal River	47.22	84.65	1773–2003	158	37	1780	0.28
Abitibi Plains east										
76	*Pinus strobus*	Gr	Hobbs Lake	46.43	80.12	1547–1994	212	31	1714	0.16
77	*Pinus resinosa*	Ce	Lac Temagami	47.00	79.00	1644–1983**	266	36	1690	0.18
78	*Populus tremuloides*	Cd	Lac Duparquet	48.28	79.19	1831–1996	146	30	1840	0.24
79	*Betula papyrifera*	Cd	Lac Duparquet	48.28	79.19	1766–1998	138	74	1804	0.25
80	*Picea mariana*	Gm	Lac Duparquet	48.28	79.19	1800–1999	126	61	1849	0.14
81	*Fraxinus nigra*	Tj	Lac Duparquet	48.28	79.19	1790–1991	100	36	1834	0.20
82	*Fraxinus nigra*	Tj	Lac Duparquet	48.28	79.19	1682–1991	134	253	1716	0.20
83	*Thuja occidentalis*	As	Lac Duparquet	48.28	79.19	1186–1987	507	46	1283	0.16
84	*Thuja occidentalis*	Tj	Lac Duparquet	48.28	79.19	1417–1987	302	43	1569	0.14
85	*Picea mariana*	Ha	Joutel	49.26	78.27	1778–1994	NA	57	NA	0.18
86	*Picea mariana*	Ha	Hedge Hills	49.16	78.24	1816–1992	NA	67	NA	0.17
87	*Picea mariana*	Ha	Chicobi Hills	48.51	78.38	1820–1994	NA	61	NA	0.16
88	*Picea mariana*	Ha	Lac Opasatica	48.06	79.18	1703–1994	NA	61	NA	0.17
89	*Picea mariana*	Ha	Lac Hébécourt	48.29	79.27	1790–1993	NA	59	NA	0.17
90	*Pinus banksiana*	By	Abitibi Lake	49.00	79.50	1713–1987	103	75	1732	0.17
91	*Pinus banksiana*	By	Lac Duparquet	48.28	79.19	1726–1985	97	94	1775	0.16
92	*Pinus banksiana*	Ha	Joutel	49.26	78.27	1714–1994	NA	51	NA	0.19
93	*Pinus banksiana*	Ha	Hedge Hills	49.16	78.24	1811–1992	NA	67	NA	0.22
94	*Pinus banksiana*	Ha	Chicobi Hills	48.51	78.38	1814–1994	NA	57	NA	0.19
95	*Pinus banksiana*	Ha	Lac Hébécourt	48.29	79.27	1776–1993	NA	49	NA	0.22
Southern Laurentian										
96	*Picea mariana*	GsDl	Lac Dionne	49.52	67.76	1809–1999	166	40	1824	0.13
97	*Picea mariana*	GsDl	Lac Dionne	49.66	67.58	1743–1999	181	48	1803	0.16
98	*Pinus banksiana*	GsDl	Lac Dionne	49.52	67.76	1811–1998	133	21	1817	0.16
99	*Abies balsamea*	KcMh	Mont Valin	48.05	70.04	1789–1994	NA	NA	NA	NA
100	*Picea mariana*	KcMh	Cote-Nord 30	49.05	69.03	1713–1996	NA	NA	NA	NA
101	*Pinus strobus*	KcGf	St-Marguerite	48.02	70.00	1768–1995	133	12	1850	0.17
102	*Picea mariana*	Sf	Lac Chevrillon	50.01	74.27	1797–1988	87	37	1813	0.14
103	*Abies balsamea*	KcMh	Lac Liberal	49.04	72.06	1751–1995	NA	NA	NA	NA

TABLE A1. *(Continued)*

	Species	Contrib-utors*	Location	Lat (°N)	Lon (°W)	Period	Mean (yr)	*N*	SSS > 0.85 (yr)	Sens
104	*Picea mariana*	Ld	Réservoir Gouin	48.56	74.30	1775–1997	116	81	1828	0.15
105	*Pinus banksiana*	Ld	Réservoir Gouin	48.56	74.30	1767–1998	74	91	1806	0.16
106	*Betula papyrifera*	Cf	Réservoir Gouin	48.56	74.30	1740–1997	147	80	1778	0.19
107	*Picea glauca*	JyMh	Lac Waswanipi	49.45	76.50	1821–1996	134	30	1848	0.16
108	*Thuja occidentalis*	JyMh	Lac des Iles	46.44	75.62	1814–1996	126	29	1863	0.15
109	*Thuja occidentalis*	JyMh	Lac Wedge	47.20	75.09	1786–1996	135	30	1845	0.19
110	*Picea glauca*	JyMh	Chibougameau	49.58	74.26	1793–1996	152	37	1829	0.20
111	*Picea glauca*	JyMh	Lac Cavan	49.75	74.97	1798–1996	161	33	1823	0.18
112	*Picea glauca*	JyMh	Lac Indiana	48.39	73.14	1749–1996	117	37	1846	0.16
113	*Picea mariana*	JyMh	Baie du Vison	48.42	74.11	1830–1996	130	29	1852	16.00
114	*Picea mariana*	JyMh	Le Canal	48.43	75.47	1811–1996	166	20	1819	0.19
115	*Picea glauca*	JyMh	Lac Bertthelot	48.54	76.13	1814–1996	127	28	1864	0.19
116	*Picea glauca*	JyMh	Lac Edouard	47.54	72.44	1846–1996	119	24	1866	0.18
117	*Picea glauca*	JyMh	Lac Kempt	47.38	74.03	1859–1996	93	35	1884	0.22
118	*Picea mariana*	JyMh	Lac du Coucou	47.58	75.58	1789–1996	144	45	1820	0.19
119	*Picea glauca*	JyMh	Rivière Cabonga	47.41	76.24	1839–1996	117	32	1880	0.19
120	*Picea glauca*	JyMh	Réservoir Dozois	47.40	77.00	1823–1996	131	25	1861	0.19
Supplemental chronologies										
121	*Picea glauca*	Sf	Mountain Lake	53.29	58.40	1709–1988	142	28	1747	0.21
122	*Picea glauca*	Sf	Churchill	58.40	93.50	1695–1988	197	26	1721	0.14
123	*Picea mariana*	Sf	Charlie Lake	60.02	100.26	1768–1988	122	26	1843	0.18
124	*Pinus strobus*	GrCb	Dividing Lake Aquatic	45.24	78.36	1950–1993	182	50	1508	0.14
125	*Picea glauca*	Dr	Nutak	57.30	61.45	1700–1996	190	10	1748	0.19
126	*Thuja occidentalis*	Ce	Sag Pond	46.80	69.20	1674–1986	246	23	1702	0.15
127	*Pinus resinosa*	KdGm	Hartwick Pines State Park	44.40	88.45	1770–1987	202	52	1778	0.18
128	*Quercus macrocapa*	MdSc	Masonic Island/Bear Island	49.00	100.30	1676–1990	167	17	1803	0.23
129	*Juniperus scopulorum*	MdSc	T. Roosevelt National Park	46.90	103.50	1597–1991	180	42	1685	0.32
130	*Larix laricina*	Mk	Churchill	58.40	93.50	1721–2000	125	71	1780	0.25
131	*Tsuga canadensis*	Ce	Bowater-Mersey	44.49	64.00	1572–1982	262	28	1637	0.22
132	*Tsuga canadensis*	Ce	Rivière Du Moulin	46.38	71.53	1524–1982	255	50	1627	0.27
133	*Thuja occidentalis*	Ce	St. Anne River	48.35	65.55	1404–1982	412	29	1475	0.13
134	*Picea mariana*	Sf	Lac Romanel	56.14	67.43	1659–1988	330	29	1743	0.12
135	*Picea mariana*	Sf	No Name Lake	54.35	77.34	1748–1988	100	31	1781	0.12
136	*Picea mariana*	Sf	No Name Lake	54.35	77.34	1743–1988	119	32	1758	0.12
137	*Picea mariana*	Sf	Lac Natuak	57.13	71.30	1743–1988	141	23	1823	0.17
138	*Picea mariana*	Sf	Eastmain River	52.02	77.51	1739–1988	164	27	1810	0.16
139	*Picea mariana*	Sf	Coats River	55.44	76.09	1777–1988	153	26	1806	0.14
140	*Picea glauca*	Jg	Castle Peninsula	56.10	76.33	1663–1982	261	35	1689	0.17
141	*Picea mariana*	Sf	Bonif, Quebec	55.20	77.50	1352–1989	116	84	1369	0.17
142	*Picea glauca*	Mk	Churchill	58.40	93.50	1646–2000	158	28	1782	0.13
143	*Picea mariana*	Mk	Churchill	58.40	93.50	1527–2000	171	69	1683	0.12
144	*Quercus alba*	Dd	Nine Eagles State Park	40.06	93.80	1672–1982	134	27	1861	0.25
145	*Tsuga canadensis*	Ce	Reed Pond	46.20	69.00	1639–1986	217	34	1729	0.26
146	*Pinus strobus*	Ce	Soper Brook West Branch	46.00	69.30	1692–1982	236	32	1711	0.15
147	*Picea rubens*	Ce	Wizard Pond	44.60	68.20	1692–1982	262	38	1709	0.14
148	*Pinus ponderosa*	WcBp	Ash Canyon	42.38	103.15	1642–1997	183	31	1738	0.33
149	*Tsuga canadensis*	Ce	Spruce Glen	41.80	74.20	1511–1984	281	31	1645	0.21
150	*Pinus ponderosa*	MdSc	Cedar Butte	43.60	101.10	1646–1991	222	16	1671	0.44
151	*Pinus ponderosa*	MdSc	Reno Gulch Pipo	43.54	103.26	1281–1991	282	32	1595	0.24
152	*Tsuga canadensis*	Ce	Bass Lake Peninsula	45.10	88.90	1595–1983	308	45	1619	0.25

* Data contributors: S. Archambault (As), Y. Bergeron (By), D. Charron (Cd), F. Conciatori (Cf), E. R. Cook (Ce), R. D'Arrigo et al. (Dr), D. N. Duvick (Dd), S. Gauthier and L. Degranpré (GsDl), M. P. Girardin (Gm), L. J. Graumlich (Gl), R. P. Guyette (Gr), R. P. Guyette and B. Cole (GrCb), A. Hofgaard (Ha), G. Jacoby et al. (Jg), Y. Jardon and H. Morin (JyMh), D. L. Koop and H. D. Grissino-Mayer (KdGm), C. Krause and H. Morin (KcMh), C. Krause and F. Gionest (KcGf), D. Lesieur (Ld), D. Meko and C. H. Sieg (MdSc), K. Monson (Mk), F. Schweingruber (Sf), S. St-Gorge (Ss), C. W. Stockton (Sc), J. Tardif (Tj), C. A. Woodhouse and P. M. Brown (WcBp).

** These two residual chronologies were increased in length by inserting the value of 1.0 (average of the residual chronology) from their latest year to present to optimize the degree of freedom (PCA rectangular matrix constraint).

APPENDIX B

List of Meteorological Stations

TABLE B1. Meteorological stations used in the calculation of the regional monthly CDC, temperature (*T*), and precipitation (*P*) variables. The period covered by each station and variable is indicated.

Stations	Code	Lat (°N)	Lon (°W)	Elevation (m MSL)	CDC	*T*	*P*
Boreal Plains							
Birtle	5010240	50.26	101.30	522	1917–95a	1904–99	1918–99
Ashern	5040120	52.08	98.22	263	1967–89	—	—
Cumberland House	4071960	53.58	102.18	271	1937–64	—	—
Dauphin	5040675	51.90	100.20	292	1890–1941	—	—
Dauphin A	5040680	51.60	100.30	305	a	1903–99	1911–99
Gilbert Plains	5040985	51.60	100.28	404	1959–98	—	—
Moosehorn	5041800	51.18	98.37	250	1910–63	—	—
Russell	5012520	50.46	101.17	567	1884–1990	1916–90*	1916–99
Swan River	5042800	52.30	101.13	347	1910–98	—	—
Lac Seul Upland and Lake of the Woods							
Dryden	6032117	49.47	92.50	372	1914–97	1914–99	1914–99
Earl Falls	6012198	50.38	93.13	361	1930–96	—	—
Fort Frances	6022475	48.37	93.25	343	1892–95	1912–99	1912–99
Great Falls	5031200	50.28	96.00	249	1923–96	1922–99	1923–99
Ignace	6033690	49.25a	91.39	447	1914–70	—	—
Indian Bay	5031320	49.37	95.12	327	1915–98	1914–99	1916–99
Kenora	6034070	49.48	94.32	336	1900–38	—	—
Kenora A	6034075	49.47	94.22	410	1939–98	1899–1999	1900–99
Red Lake A	6016975	51.40	93.48	386	1939–98	—	—
Sioux Lookout	6037775	50.70	91.54	390	1939–98	—	1914–99
Lake Nipigon							
Cameron Falls	6041109	49.90	88.21	229	1925–97	1924–98	1925–99
Geraldton A	6042716	49.47	86.56	349	1981–99	—	1950–99
Kakabeka Falls	6043930	48.24	89.37	278	1910–76	—	—
Manitouwadge	6044903	49.90	85.48	332	1956–94	—	—
Port Arthur	6046588	48.26	89.13	195	1878–41	—	—
Savanne	6047615	48.58	90.12	459	1892–46	—	—
Schreiber	6047624	48.49	87.16	302	1910–75	—	—
Thunder Bay A	6048261	48.22	89.20	199	1942–93	1895–1993	1895–1999
Abitibi Plains west							
Smokey Falls	6077845	50.40	82.10	183	1934–96	—	1934–99
Franz	6052563	48.28	84.25	373	1918–49	—	—
Hornepayne	6053570	49.12	84.46	329	1920–89	—	—
Kapuskasing	6073975	49.27	82.26	218	1937–98	—	—
Kapuskasing A	6073960	49.25	82.28	227	1919–98	1918–99	1918–99
Steep Hill Falls	6058010	48.40	84.48	335	1920–38	—	—
White River	6059475	48.36	85.17	379	1889–1975	—	—
Abitibi Plains east							
Abitibi Post	7090050	48.43	79.22	259	1898–1935	—	—
Amos	7090120	48.34	78.07	259	1915–97	1913–99	1914–99
Cochrane	6071712	49.04	81.02	275	1912–91	—	—
Duparquet	709BBDH	48.31	79.16	290	1982–93	—	—
Haileysbury	6073138	47.27	79.38	189	1895–1922	—	—
Iroquois Falls	6073810	48.45	80.40	259	1913–97	1913–99	1916–99
Kirkland Lake	6074209	48.90	80.00	324	1951–96	—	—
La Sarre	7094120	48.48	79.12	244	1952–98	—	—
Val St-Gilles	70986RN	48.59	79.07	290	1973–98	—	—
Southern Laurentian							
Albanel	7060080	48.53	72.27	152	1923–90	—	1923–99
Bagotville	7060400	48.20	71.00	159	1942–99	1895–1999	1943–99

TABLE B1. *(Continued)*

Stations	Code	Lat (°N)	Lon (°W)	Elevation (m MSL)	CDC	*T*	*P*
Barrage à Lac Kempt	7070448	47.33	74.11	421	1913–63	—	—
Barrage Gouin	7070454	48.21	74.60	404	1914–79	—	—
Chibougamau Chapais A	7091399	49.77	74.53	387	1963–98	1914–2001	1963–98*
Chicoutimi	7061441	48.25	71.50	175	1881–1979	—	—
Hemon	7063090	49.40	72.36	183	1966–98	—	—
Kenogamie	7063400	48.25	71.15	116	1924–64	—	—
La Tuque	7074240	47.24	72.47	152	1915–1998	1911–99	1912–99
Lac Bouchette	7063560	48.13	72.10	358	1951–98	—	—
Manouan Sanmaur	7074600	47.54	73.48	357	1919–72	—	—
Mistassini	7064998	48.51	72.12	122	1964–94	—	—
Mistassini Post	7095000	50.25	73.53	380	1899–80	—	—
Normandin	7065640	48.51	72.32	137	1936–92	—	1937–99
Roberval	7066688	48.32	72.14	102	1888–1965	—	1915–99
Roberval airport	7066685	48.31	72.16	179	1958–98	—	—
Tadoussac	7048320	48.15	69.72	45	1914–98	1914–99*	1914–2001

* Temperature and precipitation data obtained from Environment Canada (2000).

APPENDIX C

Mean Climatology

This paper discusses anomalies in the 500-hPa circulation with respect to the mean climatology. The mean features of the upper-atmospheric circulation are the presence of troughs located over the North Pacific [West Coast trough (WCT)] and eastern Canada [Canadian polar trough (CPT)] and a ridge over western Canada [continental ridge (CR)] (Fig. C1). The circulation and amplitudes over Canada are generally similar from month to month, but the summer gradients are much weaker than those of the winter. Also, the CR and CPT set migrates toward the east in the summer. Winds at the 500-hPa level tend to flow parallel to the height contours. The winds are called meridional when the height contours form a strong wave-like pattern, and zonal when they are nearly parallel to the lines of latitude. Within these long waves, an elongated area of high heights is known as a ridge (e.g., the CR) and an elongated area of low heights is a trough (e.g., the CPT).

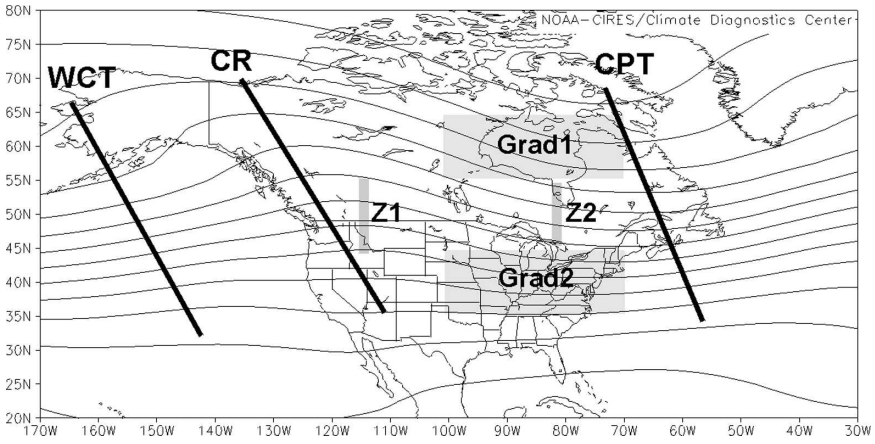

FIG. C1. Mean annual 500-hPa circulation for the reference period of 1968–96. Thick vertical lines indicate the location of the main features affecting the North American climate. From west to east these are the WCT, the CR, and the CPT. Also shown are the geographic locations of data used in the calculation of the zonal (Grad1 − Grad2) and meridional (Z1 − Z2) indices.

REFERENCES

AISN Software, 1999: AutoSignal. Version 1.5 for Windows. SPSS Inc.

Archambault, S., and Y. Bergeron, 1992: An 802-year tree-ring chronology from the Quebec boreal forest. *Can. J. For. Res.,* **22,** 674–682.

Barlow, M., S. Nigam, and E. H. Berbery, 2001: ENSO, Pacific decadal variability, and U.S. summertime precipitation, drought, and streamflow. *J. Climate,* **14,** 2105–2128.

Bergeron, Y., and S. Archambault, 1993: Decreasing frequency of forest fires in the southern boreal zone of Quebec and its relation to global warming since the end of the "Little Ice Age." *Holocene,* **3,** 255–259.

——, S. Gauthier, V. Kafka, P. Lefort, and D. Lesieur, 2001: Natural fire frequency for the eastern Canadian boreal forest: Consequences for sustainable forestry. *Can. J. For. Res.,* **31,** 384–391.

——, M. Flannigan, S. Gauthier, A. Leduc, and P. Lefort, 2004: Past, current and future fire frequency in the Canadian boreal forest: Implications for sustainable forest management. *Ambio,* **33,** 356–360.

Bonsal, B. R., and R. G. Lawford, 1999: Teleconnections between El Niño and la Niña events and summer extended dry spells on the Canadian Prairies. *Int. J. Climatol.,* **19,** 1445–1458.

——, A. K. Chakravarti, and R. G. Lawford, 1993: Teleconnections between north Pacific SST anomalies and growing season extended dry spells on the Canadian Prairies. *Int. J. Climatol.,* **13,** 865–878.

——, X. Zhang, and W. D. Hogg, 1999: Canadian Prairie growing season precipitation variability and associated atmospheric circulation. *Climate Res.,* **11,** 191–208.

Bourgeau-Chavez, L. L., M. E. Alexander, B. J. Stocks, and E. S. Kasischke, 2000: Distribution of forest ecosystems and the role of fire in the North American boreal region. *Fire, Climate Change, and Carbon Cycling in the Boreal Forest*, E. S. Kasischke and B. J. Stocks, Eds., Springer, 111–131.

Bradley, R. S., 1999: *Paleoclimatology: Reconstructing Climates of the Quaternary*. Academic Press, 613 pp.

Cook, E. R., and K. Peters, 1981: The smoothing spline: A new approach to standardizing forest interior tree-ring width series for dendroclimatic studies. *Tree Ring Bull.,* **41,** 45–53.

——, and R. Holmes, 1986: Guide for computer program ARSTAN. Laboratory of Tree-Ring Research, University of Arizona, 51 pp.

——, and L. A. Kairiukstis, 1990: *Methods of Dendrochronology: Applications in the Environmental Sciences*. Kluwer Academic, 394 pp.

——, K. R. Briffa, and P. D. Jones, 1994: Spatial regression methods in dendroclimatology: A review and comparison of two techniques. *Int. J. Climatol.,* **14,** 379–402.

——, R. D. D'Arrigo, and M. E. Mann, 2002: A well-verified, multiproxy reconstruction of the winter North Atlantic Oscillation index since A.D. 1400. *J. Climate,* **15,** 1752–1764.

D'Arrigo, R., R. Villalba, and G. Wiles, 2001: Tree-ring estimates of Pacific decadal climate variability. *Climate Dyn.,* **18,** 219–224.

Ecological Stratification Working Group, 1996: A national ecological framework for Canada. Agriculture and Agri-Food Canada and Environment Canada, Ottawa, 125 pp.

Environment Canada, 2000: *Canadian Daily Climate Data*. Canadian Climate Program, Atmospheric Environnement Service, Environnement Canada, CD-ROM.

——, cited 2002: Canadian climate normals 1971-2000. Canadian Climate Program, Atmospheric Environnement Service, Environnement Canada. [Available online at http://climate.weatheroffice.ec.gc.ca.]

Esper, J., E. R. Cook, and F. H. Schweingruber, 2002: Low-frequency signals in long tree-ring chronologies for reconstructing past temperature variability. *Science,* **295,** 2250–2253.

Evans, M. N., A. Kaplan, and M. A. Cane, 2002: Pacific sea surface temperature field reconstruction from coral δ18O data using reduced space objective analysis. *Paleoceanography*, **17,** 1007, doi:10.1029/2000PA000590.

Finney, B. P., I. Gregory-Eaves, J. Sweetman, M. S. V. Douglas, and J. P. Smol, 2000: Impacts of climatic change and fishing on Pacific salmon abundance over the past 300 years. *Science,* **290,** 795–799.

Flannigan, M. D., and J. B. Harrington, 1988: A study of the relation of meteorological variables to monthly provincial area burned by wildfire in Canada (1953-80). *J. Appl. Meteor.,* **27,** 441–452.

——, and C. E. Van Wagner, 1991: Climate change and wildfire in Canada. *Can. J. For. Res.,* **21,** 66–72.

——, and B. M. Wotton, 2001: Climate, weather, and area burned. *Forest Fires: Behavior and Ecological Effects*, E. A. Johnson and K. Miyanishi, Eds., Academic Press, 351–373.

Fritts, H. C., 2001: *Tree-Rings and Climate*. Blackburn Press, 567 pp.

——, E. A. Vaganov, I. V. Sviderskaya, and A. V. Shashkin, 1991: Climatic variation and tree-ring structure in conifers: Empirical and mechanistic models of tree-ring width, number of cells, cell-size, cell-wall thickness and wood density. *Climate Res.,* **1,** 97–116.

Gajewski, K., and D. A. Atkinson, 2003: Climatic change in northern Canada. *Environ. Rev.,* **11,** 69–102.

Gedalof, Z., D. L. Peterson, and N. J. Mantua, 2002: A multicentury perspective of variability in the Pacific Decadal Oscillation: New insights from tree rings and coral. *Geophys. Res. Lett.,* **29,** 2204, doi:10.1029/2002GL015824.

Girardin, M. P., 2005: Dendrochronological reconstruction of the variability in atmospheric circulation and fire weather conditions for the past three centuries in the Canadian boreal forest. Ph.D. dissertation, University of Manitoba, 227 pp.

——, and J. Tardif, 2005: Sensitivity of tree growth to the atmospheric vertical profile in the Boreal Plains of Manitoba. *Can. J. For. Res.,* **35,** 48–64.

——, ——, M. D. Flannigan, and Y. Bergeron, 2004a: Multicentury reconstruction of the Canadian Drought Code from eastern Canada and its relationship with paleoclimatic indices of atmospheric circulation. *Climate Dyn.,* **23,** 99–115.

——, ——, ——, B. M. Wotton, and Y. Bergeron, 2004b: Trends and periodicities in the Canadian Drought Code and their relationships with atmospheric circulation for the southern Canadian boreal forest. *Can. J. For. Res.,* **34,** 103–119.

Guiot, J., 1985: Reconstruction of seasonal temperatures and sea-level pressures in the Hudson Bay area back to 1700. *Climatol. Bull.,* **19,** 11–59.

Hofgaard, A., J. Tardif, and Y. Bergeron, 1999: Dendroclimatic response of *Picea mariana* and *Pinus banksiana* along a latitudinal gradient in the eastern Canadian boreal forest. *Can. J. For. Res.,* **29,** 1333–1346.

Holmes, R. L., 1983: Computer assisted quality control in tree-ring dating and measurement. *Tree Ring Bull.,* **43,** 69–78.

——, 1999: Documentation for programs in the dendrochronology

program library and the dendroecology program library. Laboratory of Tree-Ring Research, University of Arizona, 14 pp.

Jacobeit, J., H. Wanner, J. Luterbacher, C. Beck, A. Philipp, and K. Sturm, 2003: Atmospheric circulation variability in the North-Atlantic-European area since the mid-seventeenth century. *Climate Dyn.,* **20,** 341–352.

Jardon, Y., H. Morin, and P. Dutilleul, 2003: Périodicité et synchronisme des épidémies de la tordeuse des bourgeons de l'épinette au Quebec. *Can. J. For. Res.,* **33,** 1947–1961.

Johnson, E. A., 1992: *Fire and Vegetation Dynamics: Studies from the North American Boreal Forest*. Cambridge University Press, 143 pp.

Kalnay, E., and Coauthors, 1996: The NCEP/NCAR 40-Year Reanalysis Project. *Bull. Amer. Meteor. Soc.,* **77,** 437–471.

Knox, J. L., and R. G. Lawford, 1990: The relationship between Canadian Prairie dry and wet months and circulation anomalies in the mid-troposhere. *Atmos.–Ocean,* **28,** 189–215.

Kumar, A., and M. P. Hoerling, 2003: The nature and causes for the delayed atmospheric response to El Niño. *J. Climate,* **16,** 1391–1403.

Larsen, C. P. S., 1996: Fire and climate dynamics in the boreal forest of northern Alberta, Canada, from AD 1850 to 1989. *Holocene,* **6,** 449–456.

Latif, M., and T. P. Barnett, 1996: Decadal climate variability over the North Pacific and North America: Dynamics and predictability. *J. Climate,* **9,** 2407–2423.

Lau, K. M., J. Y. Lee, K. M. Kim, and L. S. Kang, 2004: The North Pacific as a regulator of summertime climate over Eurasia and North America. *J. Climate,* **17,** 819–833.

Legendre, P., and L. Legendre, 1998: *Numerical Ecology*. Elsevier, 853 pp.

Luckman, B. H., K. R. Briffa, P. D. Jones, and F. H. Schweingruber, 1997: Tree-ring based reconstruction of summer temperature at the Columbia Icefield, Alberta, Canada, AD 1073-1983. *Holocene,* **7,** 375–389.

Luterbacher, J., E. D. D. Xoplaki, R. Rickli, J. Jacobeit, C. B. Neck, D. Gyalistras, C. Schmutz, and H. Wanner, 2002: Reconstruction of sea leval pressure fields over the eastern North Atlantic and Europe back to 1500. *Climate Dyn.,* **18,** 545–561.

Mantua, N. J., S. R. Hare, Y. Zhang, J. M. Wallace, and R. C. Francis, 1997: A Pacific decadal climate oscillation with impacts on salmon. *Bull. Amer. Meteor. Soc.,* **78,** 1069–1079.

Meehl, G. A., and C. Tebaldi, 2004: More intense, more frequent, and longer lasting heat waves in the 21st century. *Science,* **305,** 994–997.

Mekis, E., and W. D. Hogg, 1999: Rehabilitated and analysis of Canadian daily precipitation time series. *Atmos.–Ocean,* **37,** 53–85.

Mudelsee, M., 2003: Estimating Pearson's correlation coefficient with bootstrap confidence interval from serially dependent time series. *Math. Geol.,* **35,** 651–665.

Nash, C. H., and E. A. Johnson, 1996: Synoptic climatology of lightning-caused forest fires in subalpine and boreal forests. *Can. J. For. Res.,* **26,** 1859–1874.

Newman, M., G. P. Compo, and M. A. Alexander, 2003: ENSO-forced variability of the Pacific decadal oscillation. *J. Climate,* **16,** 3853–3857.

Nigam, S., M. Barlow, and E. H. Berbery, 1999: Analysis links Pacific decadal variability to drought and streamflow in the United States. *Eos, Trans. Amer. Geophys. Union,* **80,** 621–625.

Ropelewski, C. F., and P. D. Jones, 1987: An extension of the Tahiti-Darwin Southern Oscillation. *Mon. Wea. Rev.,* **115,** 2161–2165.

Sauchyn, D. J., E. Barrow, R. F. Hopkinson, and P. Leavitt, 2002: Aridity on the Canadian Plains. *Geogr. Phys. Quat.,* **56,** 247–259.

——, J. Stroich, and A. Beriault, 2003: A paleoclimatic context for the drought of 1999-2001 in the northern Great Plains of North America. *Geogr. J.,* **169,** 158–167.

Schneider, N., A. J. Miller, and D. W. Pierce, 2002: Anatomy of North Pacific decadal variability. *J. Climate,* **15,** 586–605.

Shabbar, A., and W. Skinner, 2004: Summer drought patterns in Canada and the relationship to global sea surface temperature. *J. Climate,* **17,** 2866–2880.

Skinner, W. R., B. J. Stocks, D. L. Martell, B. Bonsal, and A. Shabbar, 1999: The association between circulation anomalies in the mid-troposphere and the area burned by wildland fire in Canada. *Theor. Appl. Climatol.,* **63,** 89–105.

——, and Coauthors, 2002: A 500-hPa synoptic wildland fire climatology for large Canadian forest fires, 1959-1996. *Theor. Appl. Climatol.,* **71,** 157–169.

Smith, T. M., and R. W. Reynolds, 2003: Extended Reconstruction of Global Sea Surface Temperatures based on COADS Data (1854–1997). *J. Climate,* **16,** 1495–1510.

Stahle, D. W., and Coauthors, 1998: Experimental dendroclimatic reconstruction of the Southern Oscillation. *Bull. Amer. Meteor. Soc.,* **79,** 2137–2152.

Stocks, B. J., and Coauthors, 2003: Large forest fires in Canada, 1959-1997. *J. Geophys. Res.*, **108,** 8149, doi:10.1029/2001JD000484.

Tardif, J., and Y. Bergeron, 1997a: Ice-flood history reconstructed with tree-rings from the southern boreal forest limit, western Québec. *Holocene,* **7,** 291–300.

——, and ——, 1997b: Comparative dendroclimatological analysis of two black ash and two white cedar populations from contrasting sites in the Lake Duparquet region, northwestern Quebec. *Can. J. For. Res.,* **27,** 108–116.

——, and ——, 1999: Population dynamics of *Fraxinus nigra* in response to flood-level variations, in northwestern Quebec. *Ecol. Monogr.,* **69,** 107–125.

——, J. J. Camarero, M. Ribas, and E. Gutiurrez, 2003: Spatiotemporal variability in tree growth in the central Pyrenees: climatic and site influences. *Ecol. Monogr.,* **73,** 241–257.

Ter Braak, C. J. F., 1994: Canonical community ordination. Part I: Basic theory and linear methods. *Écoscience*, **1,** 127–140.

——, and I. C. Prentice, 1988: A theory of gradient analysis. *Adv. Ecol. Res.,* **18,** 271–317.

——, and P. Smilauer, 1998: Canoco Reference manual and user's guide to Canoco for windows: Software for canonical community ordination (version 4). Microcomputer Power, 351 pp.

Torrence, C., and G. P. Compo, 1998: A practical guide to wavelet analysis. *Bull. Amer. Meteor. Soc.,* **79,** 61–78.

Turner, J. A., 1972: The drought code component of the Canadian forest fire behaviour system. Canadian Forest Service Publication 1316, 14 pp.

Van Wagner, C. E., 1970: New development in forest fire danger rating. Canadian Department of Fisheries and Forest, Canadian Forest Service Information Rep. PS-X-19, 37 pp.

——, 1987: Development and structure of the Canadian Forest Fire Weather Index System. Canadian Forest Service Forestry Tech. Rep. 35, 35 pp.

Vincent, L. A., and D. W. Gullett, 1999: Canadian historical and homogeneous temperature datasets for climate change analyses. *Int. J. Climatol.,* **19,** 1375–1388.

Weber, G. R., 1990: North Pacific circulation anomalies, El Niño and anomalous warmth over the North American continent in 1986-1988: Possible causes of the 1988 North American Drought. *Int. J. Climatol.,* **10,** 279–289.

Weir, J. M. H., E. A. Johnson, and K. Miyanishi, 2000: Fire frequency and the spatial age mosaic of the mixed-wood boreal forest in western Canada. *Ecol. Appl.,* **10,** 1162–1177.

Wigley, T. M. L., K. R. Briffa, and P. D. Jones, 1984: On the average of correlated time series, with application in dendroclimatology and hydrometeorology. *J. Climate Appl. Meteor.,* **23,** 201–213.

Wilson, R. J. S., and B. H. Luckman, 2003: Dendroclimatic reconstruction of maximum summer temperature from upper treeline sites in Interior British Columbia. *Holocene,* **13,** 851–861.

Woodhouse, C. A., 2003: A 431-yr reconstruction of western Colorado snowpack from tree-rings. *J. Climate,* **16,** 1551–1561.

Wu, L., and Z. Liu, 2003: Decadal variability in the North Pacific: The eastern North Pacific mode. *J. Climate,* **16,** 3111–3131.

Yamaguchi, D. K., 1991: A simple method for cross-dating increment cores from living trees. *Can. J. For. Res.,* **21,** 414–416.

Yang, H., and Q. Zhang, 2003: On the decadal and interdecadal variability in the Pacific Ocean. *Adv. Atmos. Sci.,* **20,** 173–184.

Yarnal, B., 1993: *Synoptic Climatology in Environmental Analysis: A Primer*. Belhaven Press, 195 pp.

Zhang, Y., J. M. Wallace, and D. S. Battisti, 1997: ENSO-like interdecadal variability: 1900–93. *J. Climate,* **10,** 1004–1020.